Statistical mechanics of pentagonal and icosahedral order in dense liquids

Subir Sachdev and David R. Nelson
Department of Physics, Harvard University, Cambridge, Massachusetts 02138
(Received 26 December 1984)

A Ginzburg-Landau model of short-range icosahedral order in bulk liquids, and of pentagonal order in two-dimensional fluids, is used to calculate density correlation functions in these systems. The theory predicts peaks in the structure factor, at positions determined by symmetries of ideal curved-space "crystals." The peaks are broadened in a way which reflects the inability of icosahedra and pentagons to form a close-packed lattice in flat space. The results in three dimensions provide a good fit to experiments on vapor-deposited metal films and to computer simulations.

I. INTRODUCTION

A. Theoretical background

Understanding the structure of dense liquids near the glass transition is a challenging problem. Correlations present in undercooled liquids are presumably frozen in when one drops below the glass-transition temperature T_g. The frustrated short-range order present in glasses is important, in part because it may play a role in the spectacular temperature and volume dependence of the shear viscosity and diffusion constants just above T_g. Metallic glasses, in particular, have rather sharp peaks in the structure factor.[1] The peaks are especially pronounced in one-component vapor-deposited metal films.[2–4] Conventional theories of the liquid state do not satisfactorily explain these features, particularly for single-component systems.[5] Microcrystalline models appear to be inadequate as well.[6] Although vapor-deposited films are not glasses in the traditional sense, it is believed that similar particle configurations would form if one could cool fast enough directly from the melt.[6] One does indeed find the structure factor characteristic of vapor-deposited films when cooling a Lennard-Jones liquid at the very rapid rates possible with molecular-dynamics simulations.[7]

There is growing evidence that the short-range order in simple undercooled liquids and metallic glasses is predominantly icosahedral.[8] The growing icosahedral correlations found in recent computer simulations[9] are consistent with the rise in specific heat observed experimentally in undercooled liquid metals.[10] Especially-long-range correlations in the orientations of icosahedral packing units appear[9] in large "amorphon" cluster models of structure in metallic glasses.[11] Density waves with a long-range icosahedral symmetry have been observed in rapidly cooled aluminum-manganese alloys by Shechtman *et al.*,[12] suggesting that short-range icosahedral order may be present in Al-Mn melts.

A number of authors[13–15] have argued that short-range icosahedral order can be understood by referring it to an ideal, icosahedral crystal (called polytope $\{3,3,5\}$), consisting of 120 particles embedded in the surface S^3 of a four-dimensional sphere. Regions of short-range $\{3,3,5\}$ order in most glasses are broken up by a tangled array of $-72°$ disclination lines, forced in by "frustration"—the incompatibility of flat space with a space-filling icosahedral crystal. The Frank-Kasper phases[16] of transition-metal alloys are ordered arrays of disclination lines in an icosahedral medium, rather like an Abrikosov flux lattice in a type-II superconductor. In Appendix A we review the properties of the Frank-Kasper phases, and show that the radially averaged Fourier transform of the 81-atom unit cell of $Al_{32}(Zn,Mg)_{49}$ is qualitatively rather similar to the structure factor of metallic glasses. A *disordered* network of $\pm 72°$ disclination lines provides an appealing model for structure in metallic glasses.[14]

In this paper we explore the consequences of a statistical mechanical description of frustrated short-range icosahedral order in liquids.[17] A set of order parameters $Q_{n,m_a m_b}(\mathbf{r})$ is obtained by projecting a local particle configuration onto the surface of a four-dimensional tangent sphere which can accommodate the perfect icosahedral lattice, and then expanding the projected particle density in hyperspherical harmonics[18] $Y_{n,m_a m_b}$ [see Eq. (1.5)]. The index $n=0,1,2,\ldots$ denotes different irreducible representations of SO(4) while the azimuthal quantum numbers m_a and m_b vary in integer steps in the range $-n/2 < m_a, m_b < n/2$. Only the representations $n=0,12,20,24,30,32,36,\ldots$ are allowed for particles sitting at the sites of the icosahedral lattice defined by polytope $\{3,3,5\}$.[17]

Similar order parameters can be defined in d dimensions. In two dimensions (2D), for example, we can expand particle configurations projected onto a three-dimensional sphere in the usual spherical harmonics Y_{lm} to obtain a set of order parameters $Q_{lm}(\mathbf{r})$. As discussed in Sec. II, this procedure is helpful in understanding 2D liquids with a high degree of short-range *pentagonal* order. The figure analogous to polytope $\{3,3,5\}$ is a regular icosahedron, for which only spherical harmonics with $l=0,6,10,12,\ldots$ are allowed (see Appendix C). We also show that one can obtain an order-parameter description of one-dimensional liquids by mapping particles onto a tangent disk.

Let $\mathbf{Q}_n(\mathbf{r})$ be a "vector" of order-parameter components obtained by projecting particles in d dimensions onto the surface of a tangent sphere in $d+1$ dimensions. Here, n represents an allowed irreducible representation of

$SO(d+1)$ for a $(d+1)$-dimensional Platonic solid. The azimuthal quantum numbers lead to $(n+1)^2$-component "vectors" in three dimensions and $(2n+1)$-component "vectors" in $d=2$. In Ref. 17, a Ginzburg-Landau free-energy functional of the $\mathbf{Q}_n$'s was proposed for liquids with short-range icosahedral order, namely

$$F_n=\tfrac{1}{2}\int d^dr[K_n\,|\,(\partial_\mu-i\kappa \underset{\sim}{L}{}^{(n)}_{0\mu})\mathbf{Q}_n\,|^2 + r_n\,|\,\mathbf{Q}_n\,|^2]+O(Q_n^3)\ . \tag{1.1}$$

Here the $\underset{\sim}{L}{}^n_{0\mu}$ are matrix generators of the nth irreducible representation of $SO(d+1)$. These generators rotate the plane spanned by a unit vector $\hat{\mathbf{e}}_\mu$ (in the "physical" direction μ) and a unit vector $\hat{\mathbf{e}}_0$ normal to physical space. In addition to these d generators, there are $d(d-1)/2$ additional generators denoted $\underset{\sim}{L}{}^n_{\mu\nu}$, which rotate the tangent sphere in planes (μ,ν) which keep the point of tangency fixed. The quantity κ is the inverse radius of the tangent sphere, while K_n and r_n are phenomenological coupling constants. In three dimensions, the parameter κ is related to the geodesic separation d of neighboring particles in the ideal icosahedral solid by[14]

$$\kappa d=\pi/5 \approx 0.628 \tag{1.2}$$

The physical origin of the peculiar "covariant-derivative" coupling in Eq. (1.1) is as follows. Consider two adjacent particle clusters in $d=3$, both with short-range icosahedral order. How should the centers of mass and orientations of these clusters be related? If they are orientationally mismatched, a grain boundary will appear at their interface. If they are out of registry by a translation, a stacking fault will appear. The simplest way to avoid these high-energy structures is to require that the two configurations be related by "rolling" their projections onto the tangent sphere along the path joining them. Minimizing the gradient term in (1.1) leads to a relation between the order parameter at $\mathbf{r}$ and at a neighboring position $\mathbf{r}+\boldsymbol{\delta}$,[17]

$$\mathbf{Q}_n(\mathbf{r}+\boldsymbol{\delta})=e^{i\kappa \underset{\sim}{L}{}^n_{0\mu}\delta_\mu}\mathbf{Q}_n(\mathbf{r})\ , \tag{1.3}$$

which corresponds to rolling the tangent sphere a distance δ along $\hat{\mathbf{e}}_\mu$. This rolling covariant derivative was adapted from a continuum elastic theory of glasses proposed by Sethna.[15] In Appendix B we show that a related continuum elastic theory follows from Eq. (1.1) in a low-temperature, "fixed-length" limit.

One might think, in view of Eq. (1.3), that the "vector potential" $\kappa \underset{\sim}{L}{}^n_{0\mu}$ in Eq. (1.1) could be eliminated entirely by the change of variables

$$\mathbf{Q}_n(\mathbf{r})\equiv e^{i\kappa \underset{\sim}{L}{}^n_{0\mu}r_\mu}\mathbf{Q}'_n(\mathbf{r})\ . \tag{1.4}$$

In three dimensions, this transformation implies that the order is now measured relative to a $\{3,3,5\}$ template which has been rolled in straight lines out from the origin in all directions. Contributions from the vector potential remain, however, because of the noncommutivity of the generators $\underset{\sim}{L}{}^n_{0\mu}$. Problems arise because the reference sphere will not, in general, return to its initial orientation when rolled around a closed circuit. The effect of this frustration is to force a finite density of $-72°$ wedge disclination defects into the ground state.[13–15]

Figure 1(a) shows our qualitative expectations for the phase diagram of simple fluids in $d=3$ with a high degree of short-range icosahedral order, as a function of temperature and curvature. By "curvature" we mean d/R, where R is the radius of a four-dimensional sphere on which particles with an average nearest-neighbor separation d are embedded. An elementary calculation shows that $d/R\approx 3.10/N^{1/3}$, where N is the total number of particles. As the curvature increases from zero, the frustration, together with the disclination density in the ground state, decreases until it vanishes completely for $N=120$. At high temperatures, when all the masses r_n are positive in Eq. (1.3), we have a high-temperature liquid, which can be regarded as a tangled mass of $\pm 72°$ disclination lines. At low temperatures, when the r_n's are large and negative, the ground state is a Frank-Kasper lattice of $-72°$ disclination lines. Such lattices can be defined, even for nonzero curvatures, when $N>120$.[19,20]

We expect that r_{12}, the mass corresponding to the smallest allowed value of n, changes sign at the mean-field instability temperature T_0 of the unfrustrated liquid with $N=120$. Because cubic invariants are allowed in the Landau expansion (1.1), the liquid will transform into an icosahedral crystal via a first-order phase transition[17] at temperature T_c somewhat higher than T_0. The locus of instability temperatures $T_0=T_0(d/R)$ is shown in Fig. 1(a). The frustration present for $N>120$ will depress these instability temperatures (and the corresponding first-order freezing transitions) relative to their values for $N=120$. The coupling r_{12} determines the amount of local icosahedral order, and should be insensitive to the global curvature. The depression in the instability temperature in the $N=\infty$ flat-space limit is due to the $\kappa \underset{\sim}{L}{}^{(12)}_{0\mu}$ term in Eq. (1.1).

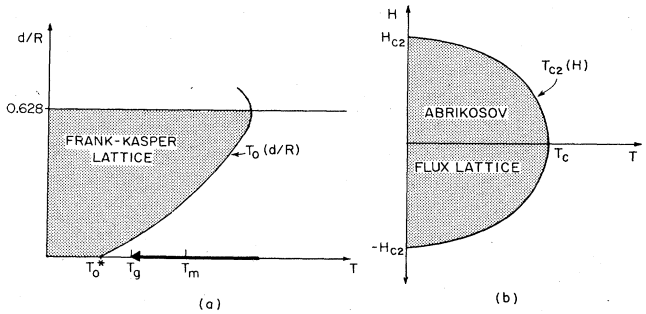

FIG. 1. (a) Hypothetical phase diagram of simple fluids with short-range icosahedral order as a function of temperature and "curvature", i.e., d/R. $T_0(d/R)$ is the mean-field instability temperature of the liquid towards a Frank-Kasper-like crystal. Its value in flat space is T_0^*. T_m is the melting temperature of a fcc lattice. The curvature $d/R=\kappa d\approx 0.628$ just accommodates polytope $\{3,3,5\}$. Since $N<\infty$, the transitions at finite curvatures will, of course, be smeared by finite size effects. (b) Phase diagram of an extreme type-II superconductor in a magnetic field. T_c is the critical temperature in the absence of a magnetic field and $H_{c2}(T)$ is the locus of transitions into an Abrikosov flux lattice.

Figure 1(a) is closely related to the phase diagram of an extreme type-II superconductor,[21] as a function of temperature and magnetic field [see Fig. 1(b)]. A locus of critical fields $H_{c2}(T)$ separates the superconducting and normal regions. As discussed in Ref. 14, unfrustrated tetrahedral particle packings on S^3 are like superconductors in zero field, and the Frank-Kasper phases in flat space are like the Abrikosov flux-lattice state. The curvature mismatch between flat space and polytope $\{3,3,5\}$ acts like an applied magnetic field. The locus of superconducting transition temperatures $T_{c2}(H)$ is like the curve of instability temperatures $T_0(d/R)$ in Fig. 1(a). In this context, it is interesting to note that the critical value of the field necessary to suppress the superconducting transition temperature to zero occurs when the cores of the Abrikosov flux vortices begin to overlap.[22] The disclination lines in the Frank-Kasper phases are separated by only two or three atomic spacings. Hence, we would expect the instability temperature in flat space, $T_0(d/R=0)\equiv T_0^*$, to be depressed far below its value in the unfrustrated 120-particle system.

The above discussion applies to liquids in (possibly metastable) thermodynamic equilibrium. To understand why Fig. 1(a) may be relevant to flat-space glass transitions, we first note that the disclination lines in the high-temperature liquid carry *non-Abelian* SU(2) matrix charges. As a result, there are strong topological barriers inhibiting line crossings at low temperatures.[14] One would expect the kinetic constraints associated with this entanglement to increase with the amount of short-range icosahedral order, becoming more and more severe as the liquid is cooled below its freezing transition T_m to, say, an equilibrium fcc crystal. Entanglement will inhibit both the transition to the fcc crystal and to a Frank-Kasper phase of ordered disclination lines. In this picture, good glass formers will drop out of equilibrium due to entanglement at a temperature $T_g < T_m$ before reaching the instability temperature T_0^* to a Frank-Kasper phase [see Fig. 1(a)].

Recent Monte Carlo simulations by Straley[23] support this view of the kinetics of glasses. Straley finds that 120 particles cooled on S^3 can easily find their $\{3,3,5\}$ ground-state configuration when annealed at temperatures somewhat below the flat-space freezing transition. Similar numbers of particles in flat space require annealing times at least 100 times longer to find the corresponding fcc ground state, even with the help of periodic boundary conditions. This difference in timescales is presumably due to the frustration and entanglement present in flat space. Since $\pm 72°$ disclinations occur in roughly equal proportions in liquids cooled on S^3, entanglement is much less important in this case.

Straley has gone on to show that the equilibrium freezing temperature of 120 particles on S^3 is about twice the flat-space fcc freezing-transition temperature T_m.[24] We expect the transition to a metastable Frank-Kasper crystal to be even lower than T_m, and that, in particular, $T_0^* \ll T_m$.

These ideas suggest that we can evaluate density correlations in a glass, or in a liquid just above T_g, by averaging over order-parameter configurations weighted by $\exp(-F/k_B T_g)$, where F is a sum of Landau free energies like Eq. (1.1). We assume timescales such that the only structural changes possible below T_g are isoconfigurational. The glass is modeled as a frozen liquid, which has dropped out of equilibrium due to entanglement. We do not deal explicitly with the dynamics of entanglement, although this was what presumably controls the dramatic behavior of transport coefficients near T_g. The entanglement kinetics we have in mind bear some resemblance to the behavior near polymer glass transitions, with disclination lines playing the role of polymers.

As a first approximation, we can truncate the expansions in Eq. (1.1) at quadratic order in $\{\mathbf{Q}_n\}$, since the large intrinsic density of defects forces these order parameters to be small. To appreciate this point more fully, imagine that the microscopic local order parameter, defined by the procedure of Ref. 17, is averaged over a volume of liquid containing several disclinations. This coarse-grained order parameter must be small, because it drops at the disclination cores, and because it adds destructively in the regions surrounding the disclinations. This point of view differs from the fixed-length continuum elastic theory of Ref. 15, which does not allow explicitly for amplitude fluctuations. For the reasons sketched above, we expect smooth variations in the amplitude of the coarse-grained order parameter whenever the averaging size exceeds the spacing between disclinations. Since the disclination network forced in by the frustration is very dense,[14] amplitude fluctuations will be important at virtually all length scales, even at temperatures near T_g.

Our approach is also different from the interesting mapping alogorithms of Sadoc and Mosseri,[19,25] who model glass structure by a literal mapping of polytope $\{3,3,5\}$ into flat space, via the introduction of disclinations. The resulting structures appear to be rather more ordered (similar to the Frank-Kasper phases) than conventional metallic glasses.[19] By appealing to the statistical mechanics of liquids in metastable equilibrium, we are, in effect, averaging over a Boltzmann-weighted ensemble of disclination configurations. Although all types of disclinations are allowed, the gradient coupling in Eq. (1.1) ensures a bias toward the $-72°$ wedge disclinations which must be present in the ground state.

B. Results and outline

In the remainder of this paper, we use the above ideas to evaluate density correlation functions in glasses.[26] The theory is a kind of unconventional microcrystalline model. Standard microcrystalline models of glass require crystallites separated by grain boundaries. In contrast, we model the structure by patches of icosahedral crystal interrupted by disclinations. In three dimensions, the order parameters $Q_{n,m_a m_b}(\mathbf{r})$ can be used to define a density on the tangent sphere at every point $\mathbf{r}$ via the relation

$$\rho(\mathbf{r},\hat{\mathbf{u}}) = \sum_{n,m_a,m_b} Q_{n,m_a m_b}(\mathbf{r}) Y^*_{n,m_a m_b}(\hat{\mathbf{u}}) \ . \tag{1.5}$$

Here, $\hat{\mathbf{u}}$ is a unit vector specifying a position on the tangent sphere. The physical particle density $\rho(\mathbf{r})$ is given by $\rho(\mathbf{r}, \hat{\mathbf{u}}=-1)$, where -1 denotes the point of tangency, which we take to be the south pole, $-1\equiv(-1,0,0,0)$. Cal-

culations of the structure factor,

$$S(q)=\langle\,|\rho(\mathbf{q})|^2\rangle\ , \tag{1.6}$$

require that we carry out Gaussian integrals over the fluctuating order-parameter fields $Q_{n,m_a m_b}(\mathbf{r})$, which in turn means diagonalizing the quadratic form defined by (1.1). The theory is similar in spirit to the Ornstein-Zernicke[27] and Cahn-Hillard[28] theories of order-parameter fluctuations near liquid-gas and binary-mixture critical points. Our calculations are more involved, however, because of the matrix character of the icosahedral order parameter. To make progress with the $(n+1)^2$-dimensional order parameters required in three dimensions, it is essential to understand and exploit fully the transformation properties of the hyperspherical harmonics under the group of four-dimensional rotations.

As discussed in Sec. III B, the theory leads to frustration-broadened peaks in the structure factor, at positions determined by the symmetries of the ideal, curved-space icosahedral crystal. The results provide a good fit to experiments on single-component amorphous-metal films,[2–4] which exhibit peaks corresponding to the icosahedral representations $n=12$, 20, and 24, and an additional peak which appears to be a composite of $n=30$ and 32 [see Figs. 8(a), 8(b), and Table III]. Upon estimating the effect of the nonlinearities in Eq. (1.1), we find that the $n=24$ peak is moved closer to the experimentally observed position, with much smaller shifts in the remaining peaks.

The peak heights and widths are used to fit the phenomenological Landau parameters r_n and K_n appearing in Eq. (1.1). The relative peak positions, however, are a consequence of the theory. All the r_n's turn out to be negative, suggesting a high degree of short-range icosahedral order. These systems are characterized by a temperature which is well below the temperature at which 120 particles would order on the surface of a 4D sphere. The Gaussian theory is stabilized, despite these negative masses, by the frustrated gradient couplings.

The theory also gives a good description of the structure factor of "computer glasses," formed when liquids interacting with simple pair potentials are cooled at the very rapid rates possible with molecular-dynamics simulations.[7] The single-component amorphous metals discussed above are not glasses in the conventional sense, because they are made by deposition from the vapor, rather than by cooling the melt. Binary metallic glasses *can* be prepared from the melt, and exhibit peaks in $S(q)$ which are broadened relative to single-component systems.[1] By allowing for an additional, fluctuating-composition variable, we can easily account for these more common metallic glasses.

Some of these ideas may be applicable to other kinds of glassy materials. Organic glass formers,[29] for example, are made with bulky molecules like toluene. It is possible that the awkward molecular shape serves mainly to slow down the kinetics, and that the centers of mass will be correlated in a way similar to the particle positions in a metallic glass. To our knowledge, the careful diffraction measurements necessary to test this hypothesis have not been done.

It may also be possible to apply curved-space models to amorphous semiconductors. One appealing candidate for describing tetrahedrally coordinated structures is "polytope 240,"[25] which is a regular lattice of 240 particles arranged in six-membered boat-shaped rings inscribed on S^3. Particle configurations with short-range polytope-240 order are also characterized by nonzero hyperspherical harmonics with $n=12,20,24,\ldots$. We have found that the theory constructed here does a poor job in explaining the experimentally observed peak positions in vapor-deposited amorphous Ge,[30] although there is somewhat better agreement is found for III-V compound semiconductors.[31,32] The discrepancy with a-Ge may be due to odd-membered rings, which are absent in polytope 240, and suppressed energetically in III-V compounds. One additional complication is that there are actually two chiral variants of polytope-240.[33] Consequently, one might expect the short-range order in semiconductors to be disrupted by domain walls separating regions of different chirality, as well as by disclination lines. We have examined the Connell-Temkin model[32] of III-V compounds, which is a hand-built tetrahedral random network, made of only even-membered rings. The model consisted of one large region (90% of the atoms) of *right*-handed polytope-240 short-range order, separated from a small region of left-handed polytope-240 order by a domain wall. The model contains eight- as well as sixfold rings; most of the eightfold rings are concentrated in the domain wall.

In Sec. II we discuss density correlations in uniformly frustrated Ginzburg-Landau models of liquids in one and two dimensions. The two-dimensional model describes fluids with a high degree of short-range pentagonal order using a template which is a regular icosahedron. The mathematical apparatus necessary to obtain results in three dimensions is described in Sec. III. The effect of nonlinearities is treated in Sec. III D. In Appendix A we review the architecture of the Frank-Kasper phases and their relationship to the theories discussed in this paper. In Appendix B we discuss the behavior of the theory in a low-temperature fixed-length limit. The selection rules for ordinary spherical harmonics projected onto the icosahedral point group are worked out in Appendix C.

II. LOW-DIMENSIONAL MODELS

In this section we study low-dimensional analogs of the "rolling-sphere" model. Their mathematical simplicity and the ease of visualization will add additional insight to our analysis of icosahedral ordering in three dimensions.

A. One dimension

We examine the theory of a liquid of particles constrained to move along a line, with interactions favoring a mean interparticle spacing d. The ground state of such a system is obvious: the particles are regularly spaced a distance d apart. At any finite temperature, however, thermal fluctuations destroy this ordering.[34] We attempt to describe the statistical mechanics of this system using an ideal template consisting of a circle inscribed with p regularly spaced particles. This "Platonic disk" plays a role similar to the solids discussed in the Introduc-

tion. The label p distinguishes between the infinite number of ideal polytopes that could be used in one dimension. The inverse radius κ of the disk must clearly satisfy the relation

$$\kappa d = 2\pi/p \ . \tag{2.1}$$

In the limit $p \to \infty$, we recover the conventional reference lattice for phonon displacements in a one-dimensional crystal.

The representations of U(1), the symmetry group of the disk, are one dimensional, the representation m being generated by the function $e^{im\theta}$, where θ is an angular coordinate on the disk. The representations which are invariant under the symmetry operations of the Platonic disk of p particles are given by $m = jp$, where j is an integer. We now project density fluctuations on the line onto a featureless tangent disk of radius κ^{-1}, and expand the projected density in the basis functions of these irreducible representations. Although all values of m are possible in a disordered-particle configuration, we expect that short-range crystalline order will give rise to large Fourier components for $m = 0, \pm p, \pm 2p, \ldots$. Accordingly, we approximate the statistical mechanics of the partially ordered liquid by restricting our attention to the special Fourier components,

$$\psi_m(x) = \frac{1}{2\theta_0} \int_{-\theta_0}^{\theta_0} d\theta \, e^{-im\theta} \rho_x'(\theta), \quad m = 0, \pm p, \pm 2p, \ldots \ . \tag{2.2}$$

Here $\rho_x'(\theta)$ is the projection of the particle density onto the disk at the point x, and $\pm\theta_0$ denotes the boundary of the projected averaging "volume." (See Fig. 2.)

We can use these Fourier components to define a density $\rho(x,\theta)$ which depends on both position x and the angular coordinate θ of the Platonic disk,

$$\rho(x,\theta) \equiv \sum_{m=0,\pm p,\ldots} \psi_m(x) e^{im\theta} \ . \tag{2.3}$$

The flat-space particle density is $\rho(x) \equiv \rho(x,\theta=0)$. A Ginzburg-Landau expression for the free energy in terms of the order parameters $\psi_m(x)$ reads

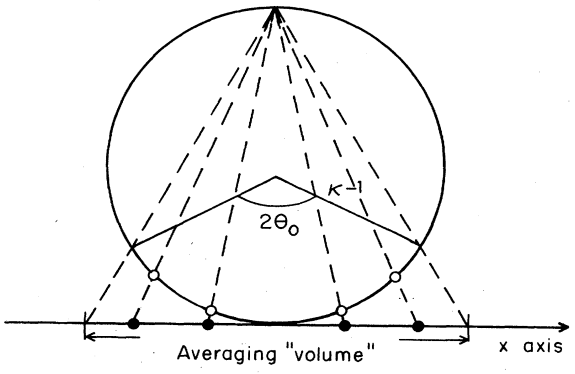

FIG. 2. Schematic showing the projection of a configuration of particles along a line onto a tangent disc. θ_0 is the angle over which an integration is performed to define the order parameter.

$$F = \tfrac{1}{2} \sum_{m=0,\pm p,\ldots} \int_{-\infty}^{\infty} [K_m \, | (\partial_x - i\kappa m)\psi_m \, |^2 + r_m \, | \psi_m \, |^2] dx + O(\, | \psi_m \, |^4) \ . \tag{2.4}$$

The K_m's are elastic constants and the r_m's are temperature-dependent masses. The form of the gradient term ensures that it will be minimized when $\psi_m(x+\delta) = e^{i\kappa m\delta}\psi_m(x)$. The same phase relationship between Fourier modes would be obtained for particles deposited on the x axis by rolling the p-fold reference Platonic disk from x to $x+\delta$. In terms of the Fourier-transformed order parameter

$$\psi_m(q) \equiv \int_{-\infty}^{\infty} \psi_m(x) e^{iqx} dx \ , \tag{2.5}$$

the Gaussian part of the free energy (2.4) becomes

$$F = \tfrac{1}{2} \sum_{m=0,\pm p,\ldots} \sum_{q} \, | \psi_m(q) \, |^2 [K_m(q-\kappa m)^2 + r_m] \ . \tag{2.6}$$

At high temperatures, fluctuations restrict the magnitude of $\psi(\mathbf{r})$, and truncation of the free energy at quadratic order will be a good approximation. Alternatively, we can work with a small order parameter by coarse-graining the $\{\psi_m(\mathbf{r})\}$ over a flat space of average size L large compared to the transitional correlation length $\xi(T)$. This restricts the allowed q values in (2.6) to $q \lesssim L^{-1}$. The structure factor $S(q)$ of this system can now easily be calculated from the equipartition theorem,

$$S(q) = \langle \, | \rho(q) \, |^2 \rangle = \sum_m \frac{k_B T}{K_m(q-\kappa m)^2 + r_m} \ . \tag{2.7}$$

This structure factor is a series of Lorentzians with peak positions at $q_m = \kappa m$ and temperature-dependent widths determined by the r_m's. The peaks occur at precisely the positions of the reciprocal-lattice vectors of the ordering at zero temperature.

Although pedagogically interesting, this system is of course unfrustrated. This can be seen in two ways: (a) The eigenvalue of the gradient term, i.e., $K_m(q-\kappa m)^2$, goes to zero at $q = \kappa m$, which means that the corresponding coupling in Eq. (2.4) can be made to vanish. (b) If we make a gauge transformation of the order parameter [analogous to Eq. (1.4)]

$$\psi_m(x) = \psi_m'(x) e^{im\kappa x} \ , \tag{2.8}$$

the free-energy density becomes

$$F = \sum_m \tfrac{1}{2} (K_m \, | \partial_x \psi_m' \, |^2 + r_m \, | \psi_m' \, |^2) \ . \tag{2.9}$$

We are left with the standard Landau gradient coupling. Variations in the phase of $\psi_m(x)$ now correspond to the small phonon displacements entering conventional continuum elastic theories.

B. Pentagonal order in two dimensions

Frustration *does* appear in two-dimensional liquids with interactions that strongly favor fivefold coordina-

tion. Although it is impossible to make a lattice of particles which is everywhere five-coordinated in the plane, twelve particles, each having five nearest neighbors, *can* be accommodated on the surface S^2 of a sphere in three dimensions.[35] The centers of the particles form a regular icosahedron which plays a role similar to polytope $\{3,3,5\}$ in three-dimensional packings. If the great circle distance between the particles on S^2 is d, it is straightforward to show using the geometry of an icosahedron[36] that

$$\kappa d = \cos^{-1}\frac{\sqrt{5}}{5} \approx 1.11 , \tag{2.10}$$

where κ is the inverse radius of the sphere.

Comparison with the corresponding result (1.2) for polytope $\{3,3,5\}$ shows that this system is considerably more frustrated. Figure 3 shows a high-density configuration of particles obtained by annealing small aluminum pentagons in a vibrating-dish apparatus.[37] These pentagons would form a regular dodecahedron on S^2. Note that essentially *every* particle is six-coordinated, and that the centers of the pentagons appear to form a hexagonal-close-packed lattice! This result is less surprising when we remember that the average coordination number $\overline{Z}$ in a plane is constrained topologically to be six,[38] regardless of the form of the interparticle potentials. We may also think of the six-coordinated sites as $-72°$ disclinations in the twelve-atom reference "crystal" discussed in the preceding paragraph. We would expect that the frustration of pentagonal order in flat space could be accommodated by a regular Frank-Kasper lattice of point disclinations. It is evident from Fig. 3 that the large frustration forces virtually all particles to sit on defect sites.

The high defect density makes a regular icosahedron a slightly awkward template for describing order in the plane. Nevertheless, this point of view provides a useful testing ground for the theoretical ideas used to make more substantive predictions in Sec. III. The approach does surprisingly well in predicting the positions of the peaks of the structure factor associated with the sixfold order in Fig. 2.

The symmetry group of S^2 is SO(3). Its irreducible representations, labeled by a non-negative integer l, are generated by the spherical harmonics $Y_{lm}(\hat{\mathbf{u}})$. Here, $\hat{\mathbf{u}}=\hat{\mathbf{u}}(\theta,\phi)$ is a unit vector parametrizing S^2. Just as in one dimension, we can project the particles in the plane around the point $\mathbf{r}=(x,y)$ onto S^2. The radius of this tangent sphere should be chosen to satisfy Eq. (2.10), where d is the geodesic interparticle spacing of the projected pentagons. As shown in Appendix C, only the representations $l=0,6,10,12,15,16,\ldots$ are allowed for particles on S^2 with an icosahedral symmetry. We make the approximation that only these modes appear when we expand the projected particle density in spherical harmonics. From the projected particle density $\rho_{\mathbf{r}}(\hat{\mathbf{u}})$ we can define an order parameter $Q_{lm}(\mathbf{r})$ given by

$$Q_{lm}(\mathbf{r}) = \int_{\Delta S} \rho_{\mathbf{r}}(\hat{\mathbf{u}}) Y^*_{lm}(\hat{\mathbf{u}}) d\hat{\mathbf{u}}$$

integrating over a small region ΔS around the point $\mathbf{r}$. The resulting expansion coefficients $Q_{lm}(\mathbf{r})$ can be used to define a density on all of S^2 at every point $\mathbf{r}$, namely

$$\rho(\mathbf{r},\hat{\mathbf{u}}) \equiv \sum_{l=0,6,10,\ldots} \sum_{m=-l}^{l} Q_{lm}(\mathbf{r}) Y_{lm}(\hat{\mathbf{u}}) . \tag{2.11}$$

Let us take the point of tangency of S^2 and R^2 to be the south pole $\hat{\mathbf{u}}=\hat{\mathbf{u}}_0=(0,0,-1)$. Since

$$Y_{lm}(\hat{\mathbf{u}}_0) = (-1)^l \left[\frac{2l+1}{4\pi}\right]^{1/2} , \tag{2.12}$$

the physical particle density is given by

$$\rho(\mathbf{r}) = \rho(\mathbf{r},\hat{\mathbf{u}}_0) = \sum_{l=0,6,10,\ldots} \left[\frac{2l+1}{4\pi}\right]^{1/2} Q_{l0}(\mathbf{r})(-1)^l . \tag{2.13}$$

To determine the form of the gradient coupling in a Landau expansion in the order parameters $\{Q_{lm}(\mathbf{r})\}$, we require that $\rho(\mathbf{r}+\boldsymbol{\delta},\hat{\mathbf{u}})$ be obtained by rolling the density on the sphere at $\mathbf{r}$ along the vector $\boldsymbol{\delta}$. Consider for concreteness the case $\boldsymbol{\delta}=(\delta,0)$. Then we demand that

$$\rho(x+\delta,y,\hat{\mathbf{u}}) = \rho(x,y,\underset{\sim}{R}_{\hat{\mathbf{y}}}(-\kappa\delta)\hat{\mathbf{u}}) , \tag{2.14}$$

where $\underset{\sim}{R}_{\hat{\mathbf{n}}}(\theta)$ rotates $\hat{\mathbf{u}}$ by an amount θ about the n axis. Equation (2.14) will be consistent with Eq. (2.11) for small δ provided

$$\partial_x Q_{lm} = -i\kappa(\underset{\sim}{L}{}^{(l)}_{y})_{m\bar{m}} Q_{l\bar{m}} . \tag{2.15}$$

We have used the summation convention, and denoted by $\underset{\sim}{L}{}^{(l)}_{i}$ the $(2l+1)\times(2l+1)$ matrix generator of rotations about the i direction, acting on the lth representation of SO(3). A similar analysis of rolling in the y direction leads us to a free energy with a gradient term that minimizes the density difference between points on the plane and nearby points on the spheres, namely

$$F = \tfrac{1}{2} \sum_{l=0,6,10,12,\ldots} \int d^2\mathbf{r}[K_l \,|\, (\partial_\mu + i\kappa\epsilon_{\mu\nu}\underset{\sim}{L}{}^{(l)}_{\nu})\mathbf{Q}_l \,|^2 + r_l \,|\, \mathbf{Q}_l \,|^2] + O(\mathbf{Q}^3) . \tag{2.16}$$

Here, $\mathbf{Q}_l$ represents the $(2l+1)$-component vectors Q_{lm}, and the sums over (μ,ν) extend over (x,y). Again the K_l's are elastic constants and the r_l's are temperature-dependent masses. The quantity $\epsilon_{\mu\nu}$ is the 2×2 antisymmetric tensor with $\epsilon_{xy}=1$.

The free energy (2.16) is frustrated, in much the same way as the corresponding description of $\{3,3,5\}$ order in three dimensions.[17] To see this, consider what happens when we try to minimize the gradient term around the small plaquette shown in Fig. 4. The gradient energy will be minimized along a line connecting two neighboring points provided

$$\mathbf{Q}_l(\mathbf{r}+\boldsymbol{\delta}) = e^{-i\kappa\epsilon_{\mu\nu}L_\nu\delta_\mu}\mathbf{Q}_l(\mathbf{r}) . \tag{2.17}$$

Here, and henceforth, we drop the representation index on the generator $\mathbf{L}$ for simplicity. Adding up the changes caused by traversing the plaquette with edge length a in Fig. 4, we obtain

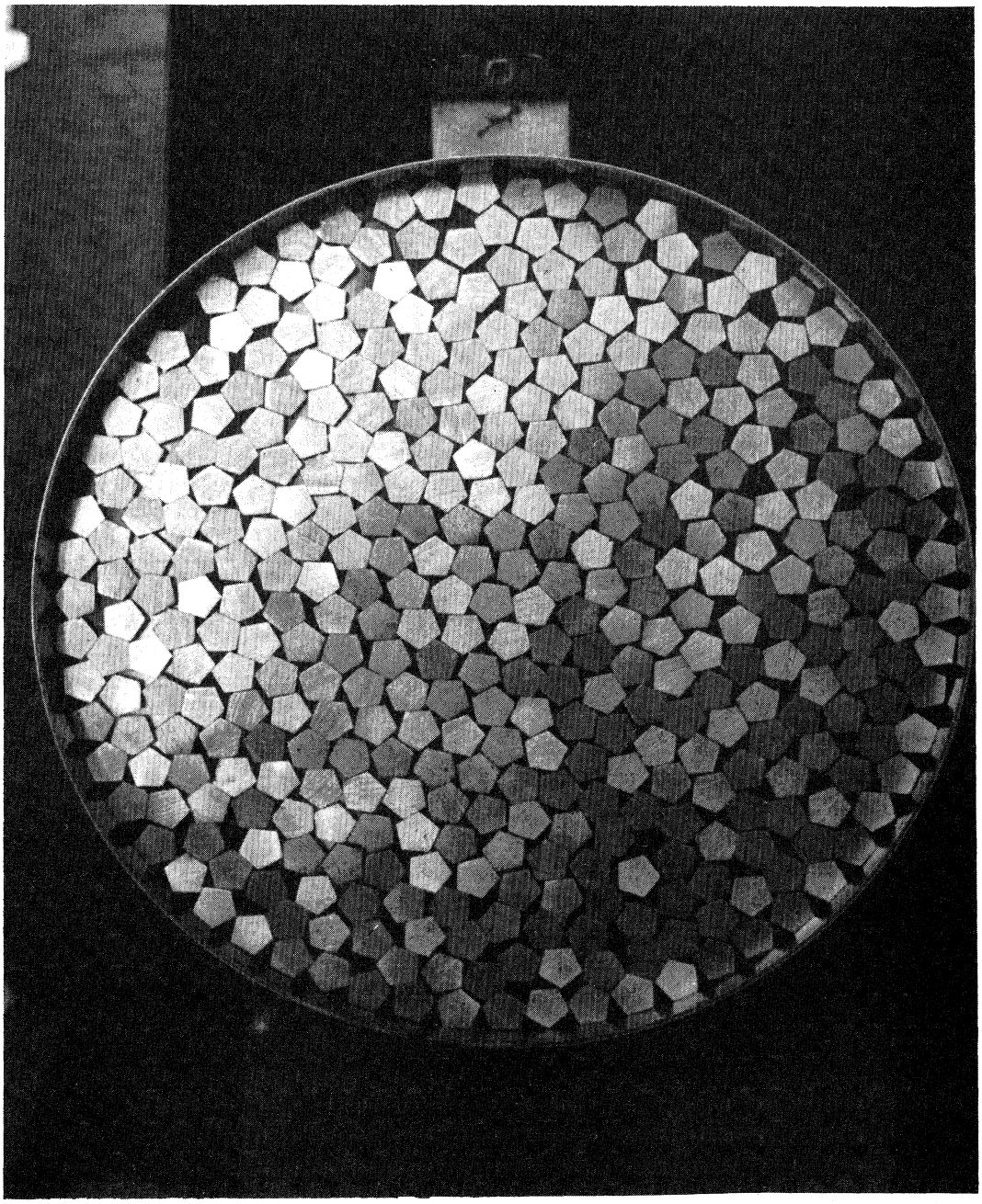

FIG. 3. Snapshot of a configuration obtained by "annealing" a high-density "liquid" of small aluminum pentagons. This configuration was obtained by gradually increasing the density of pentagons in a vibrating-shake-table apparatus (Ref. 37).

$$\begin{aligned}\mathbf{Q}_l(\mathbf{r}) &\rightarrow e^{-i\kappa \underset{\sim}{L}_y a} e^{i\kappa \underset{\sim}{L}_x a} e^{i\kappa \underset{\sim}{L}_y a} e^{-i\kappa \underset{\sim}{L}_x a} \mathbf{Q}_l(\mathbf{r}) \\ &\approx [1-(\kappa a)^2 [\underset{\sim}{L}_x, \underset{\sim}{L}_y]] \mathbf{Q}_l(\mathbf{r}) \\ &\approx e^{-i(\kappa a)^2 \underset{\sim}{L}_z} \mathbf{Q}_l(\mathbf{r}) \ . \end{aligned} \tag{2.18}$$

We see that the order parameter will not in general return to its initial value, and has instead been rotated about the z axis by an amount proportional to the area of the plaquette. This frustration can be accommodated provided the plaquette contour encircles an integral number of $-72°$ wedge disclinations.

We will now use this free energy to calculate the structure factor of a disordered liquid of hard-disk pentagons in two dimensions. Because of the frustration we expect pentagonal ordering to be small, so it may be reasonable to truncate the free energy at quadratic order in the Q_{lm}'s. It follows from Eq. (2.13) that the structure function is given in terms of the Fourier transforms $\rho(\mathbf{q})$ and $Q_{lm}(\mathbf{q})$ by

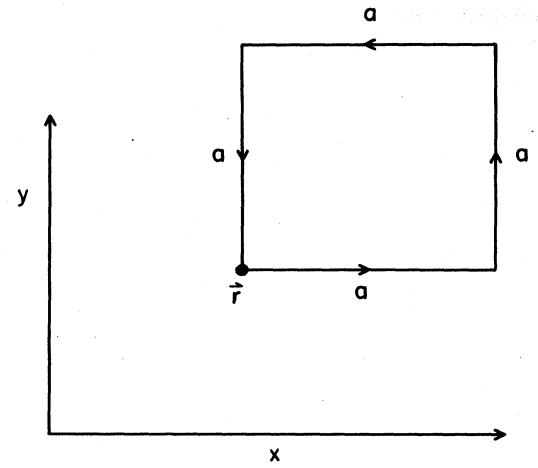

FIG. 4. Elementary plaquette along which the sphere is rolled. The order parameter at r is rotated from the order parameter obtained by traversing the plaquette.

$$S(q)=\langle\,|\rho(\mathbf{q})|^2\rangle = \sum_{l=0,6,10,\ldots}\frac{2l+1}{4\pi}\langle\,|Q_{l0}(\mathbf{q})|^2\rangle\ . \tag{2.19}$$

To calculate these averages, we Fourier-transform the free energy (2.16), and note that we need to diagonalize the quadratic form

$$Q^*_{lm_1}(\mathbf{q})\Xi_{m_1m_2}(\mathbf{q})Q_{lm_2}(\mathbf{q})\ , \tag{2.20a}$$

where the $\Xi_{m_1m_2}$ are the matrix elements of

$$\Xi=q^2+2\kappa\epsilon_{\mu\nu}q_\mu L_\nu+\kappa^2(L_x^2+L_y^2)\ . \tag{2.20b}$$

It is tedious, but straightforward, to show that both the eigenvalues and eigenvectors of Ξ are independent of the direction of $\mathbf{q}$ in the (x,y) plane. Taking for concreteness, $\mathbf{q}=(q,0)$, we note that Ξ can be rewritten

$$\Xi(q)=q^2+2\kappa qL_y+\tfrac{1}{2}\kappa^2L^2+\tfrac{1}{2}\kappa^2L_y^2+\frac{L_x^2-L_z^2}{2}\kappa^2\ . \tag{2.21}$$

The first four terms are diagonal in an (unconventional) "angular momentum" basis set $|\,lm\,\rangle$, such that[39]

$$L_y\,|\,lm\,\rangle=m\,|\,lm\,\rangle,\quad m=-l,\ldots,+l \tag{2.22a}$$

$$L^2\,|\,lm\,\rangle=l(l+1)\,|\,lm\,\rangle\ , \tag{2.22b}$$

$$L_\pm\,|\,lm\,\rangle=\sqrt{(l\mp m)(l\pm m+1)}\,|\,l,m\pm1\,\rangle\ , \tag{2.22c}$$

where

$$L_\pm=L_z\pm iL_x\ . \tag{2.23}$$

Using this basis and defining $\beta\equiv q/\kappa$, we can rewrite (2.21) as

$$\kappa^{-2}\Xi(\beta)=\beta^2+2\beta m+\tfrac{1}{2}l(l+1)+\tfrac{1}{2}m^2-\tfrac{1}{4}(L_+L_++L_-L_-)\ . \tag{2.24}$$

The last two terms of Eq. (2.24) couple different m indices, and have to be diagonalized. Note that these off-diagonal terms only mix together the odd-m and the even-m subspaces separately. For large values of β the diagonal terms dominate and we can treat the off-diagonal terms as a perturbation. The eigenvalues to order $1/\beta$ are $\kappa^{-2}\lambda_m(\beta)$, where

$$\lambda_m(\beta)=\beta^2+2m\beta+\frac{l(l+1)}{2}+\frac{m^2}{2}+\frac{1}{16}\frac{(l+m)(l-m+1)(l+m-1)(l-m+2)}{4\beta+2m+2}-\frac{1}{16}\frac{(l-m)(l+m+1)(l+m+2)(l-m-1)}{4\beta+2m+2}\ . \tag{2.25}$$

This expression has a minimum as a function of β at

$$\beta\approx-m\ . \tag{2.26}$$

The lowest eigenvalue occurs for $m=-l$ and is given by

$$\lambda_{-l}(l)=\tfrac{1}{2}l-\frac{1}{8}\frac{l(2l+1)}{(l+1)}\ . \tag{2.27}$$

The eigenvalues can also be determined for small values of β. Again taking $\mathbf{q}=(q,0)$, but returning to a quantization scheme along the z axis, we can rewrite Eq. (2.20) as

$$\kappa^{-2}\Xi(q)=\beta^2+L^2-L_z^2+2\beta L_y=\beta^2+l(l+1)-m^2+2\beta L_y\ . \tag{2.28}$$

The off-diagonal terms are now negligible for small values of β. The eigenvalues are doubly degenerate for $\beta=0$ but the degeneracy splits for nonzero values of β. Up to order β^2 the eigenvalues of Ξ are given by $\kappa^{-2}\lambda_m(\beta)$, with

$$\lambda_m(\beta)=\beta^2+l(l+1)-m^2+\beta^2\frac{(l+m+1)(l-m)}{2m+1}-\beta^2\frac{(l+m)(l-m-1)}{2m-1}\ , \tag{2.29}$$

where m refers to a different basis set than in Eq. (2.25). The eigenvalues decrease quadratically with β for all m and no minimum is in sight.

It is straightforward to diagonalize the quadratic form on a computer. A plot of all the eigenvalues as a function of β for $l=6$ is shown in Fig. 5. Table I shows the minimum eigenvalues and the values of β for which it occurs. We find the large-β perturbation theory gives a good estimate of the size and position of this minimum. Let us denote the ith eigenvalue for a given l by $\lambda_l^i(q)$. The eigenvalues are ordered such that $\lambda_l^i(q)$ is a monotonically increasing function of i and $1\le i\le 2l+1$. Note that all the eigenvalues are bounded below by a positive constant. This is a consequence of the frustration inherent in the packing of pentagons in the plane. It is impossible to make the gradient term in Eq. (2.16) vanish identically.

After carrying out a unitary transformation to the eigenvalues of $\Xi(q)$, the free energy (2.16) may be written

$$F=\tfrac{1}{2}\sum_{l=0,6,\ldots}\sum_{i=1}^{2l+2}\sum_{\mathbf{q}}|\,\alpha_l^i(\mathbf{q})\,|^2[K_l\lambda_l^i(q)+r_l]\ , \tag{2.30}$$

where $\alpha_l^i(\mathbf{q})$ is a variable measuring the strength of the ith

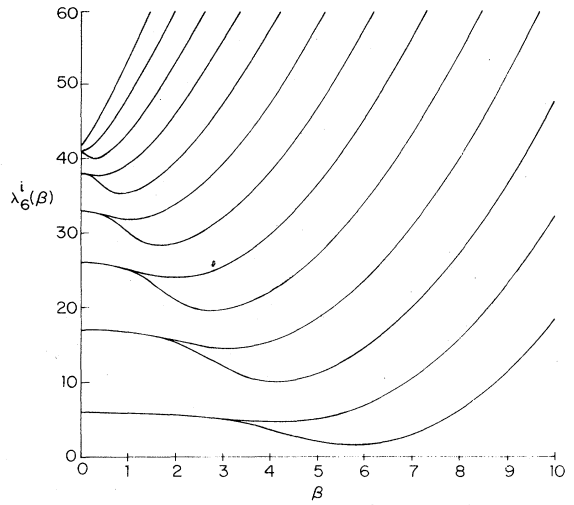

FIG. 5. A plot of the eigenvalues of the gradient part of the quartic free energy describing pentagonal ordering in two dimensions. The eigenvalues are shown for the $l=6$ representation.

eigenmode. Writing

$$Q_{lm}(\mathbf{q})=\sum_{i=1}^{2l+1}\alpha_l^i(\mathbf{q})e_{lm}^i(\mathbf{q})\ , \tag{2.31}$$

where $e_{lm}^i(\mathbf{q})$ denotes the components of the ith eigenvector in a basis quantized along the z axis, we see from Eq. (2.19) that

$$S(q)=\sum_{l=0,6,\ldots}\frac{2l+1}{4\pi}\sum_{i,j}\langle\alpha_l^i(\mathbf{q})\alpha_l^j(-\mathbf{q})\rangle e_{l0}^i(\mathbf{q})e_{l0}^j(-\mathbf{q})$$
$$=\sum_{l=0,6,\ldots}\frac{2l+1}{4\pi}\sum_{i=1}^{2l+1}\frac{k_BT}{K_l\lambda_l^i(q)+r_l}\sum_i|e_{l0}^i(\mathbf{q})|^2\ . \tag{2.32}$$

In the last step, we have used the equipartition theorem and the normal-mode decomposition (2.30).

It is straightforward to check that the eigenvectors are only weak functions of q, so that the dominant wave-vector dependence in $S(q)$ comes from the eigenvalues displayed in Fig. 5. Assuming that the lowest eigenmode dominates, we see that there will be one peak in $S(q)$ for every allowed value of l. Table I shows the peak positions, relative to the first peak, assuming these are given by the minimum in the smallest eigenvalue. Also shown are these ratios as determined by estimating a root-mean-square wave vector q_l on S^2 associated with lth-rank spherical harmonics. This can be done by averaging $|\nabla Y_{lm}|^2$ over S^2, to obtain

$$q_l^2\equiv\kappa^2\int d\Omega_{\hat{\mathbf{u}}}|\nabla Y_{lm}(\hat{\mathbf{u}})|^2$$
$$=\kappa^2 l(l+1)\ . \tag{2.33}$$

Finally, we show the Bragg vectors of a 2D hcp crystal, divided by the smallest Bragg vector q_0. The magnitudes of these Bragg vectors are presumably a good approximation to the peak positions of the structure function of any liquid with hexagonal interparticle correlations, as is the case for the pentagons in Fig. 3.

The Gaussian approximation is meant to be a good description of a *disordered* liquid of defects. We would not expect the ratio of the positions of minimum eigenvalues to match exactly with the ratios of the Bragg peaks of the hcp lattice. Nevertheless the Gaussian approach does appear to work rather well for the first three peaks in the structure factor.

III. ICOSAHEDRAL ORDER IN THREE DIMENSIONS

A. Gaussian free energy

We now study icosahedral order in three dimensions. As stated earlier, because of the impossibility of tiling flat space with icosahedra, one looks for ideal tessalations in a curved space. On the surface of a sphere in four dimensions (S^3) there exists a polytope of icosahedrally coordinated particles—polytope $\{3,3,5\}$. The strategy, in keeping with the ideas developed in Sec. II, is to associate a tangent sphere with each point in flat space and minimize the density difference between flat space and the sphere.

We need to develop a convenient coordinate system on the sphere, and analyze the representations of SO(4) and their transformation properties. We use the well-known isomorphism[18] between S^3 and SU(2) to represent points on S^3 by 2×2 unitary matrices with unit determinant. A convenient parametrization of the point $\hat{\mathbf{u}}$ is

$$\hat{\mathbf{u}}\rightarrow u=w+i\mathbf{r}\cdot\boldsymbol{\sigma}=\begin{bmatrix}w+iz & ix+y\\ ix-y & w-iz\end{bmatrix},\quad \hat{\mathbf{u}}\equiv(w,x,y,x) \tag{3.1}$$

TABLE I. Relative peak positions in the structure factor of a 2D pentagonal liquid. The fourth column is the theoretical prediction, which should be compared to the result for a hcp lattice of pentagons (see Fig. 3) in the last column. The fifth column is the prediction which follows from Eq.(2.33).

l	$\beta_{\min}(l)$	$\lambda(\beta_{\min})$	$\beta_{\min}(l)/\beta_{\min}(6)$	q_l/q_6	q_{hcp}/q_0
6	5.77	1.69	1	1	1
10	9.67	2.45	1.68	1.62	1.73
12	11.63	2.78	2.02	1.93	2.00
15	14.57	3.26	2.53	2.39	2.65
16	15.55	3.41	2.69	2.54	3.00

where σ is the vector of Pauli matrices, and [setting $\mathbf{r}=(x,y,z)$]

$$w^2+\mathbf{r}^2=1 \ . \tag{3.2}$$

Henceforth, we shall think of a point on S^3 both as a four-vector and as an SU(2) matrix.[40] We shall denote a point by $\hat{\mathbf{u}}$ when we want to use four-vector notation, and simply write u when we mean an SU(2) matrix. Rolling of S^3 in this coordinate system is straightforward to parametrize. We use the fact that the geodesic distance s between the points u and v [regarded as SU(2) matrices] is given by

$$\kappa s=\cos^{-1}[\tfrac{1}{2}\mathrm{Tr}(uv^{\dagger})] \ , \tag{3.3}$$

where κ^{-1} is the radius of the sphere. Let $\hat{\mathbf{u}}_0=-(-1,0,0,0)$ be the point of tangency of a sphere placed at the origin of flat space. In SU(2) notation, this point corresponds to minus the identity matrix. If we roll S^3 from the origin along the direction $\hat{\mathbf{r}}$, then the point on S^3 which will roll onto the point $\mathbf{r}$ will be

$$\begin{aligned} u&=\cos(\kappa r)+i\hat{\mathbf{r}}\cdot\sigma\sin(\kappa r) \\ &=e^{i\kappa(\mathbf{r}\cdot\hat{\sigma})} \ . \end{aligned} \tag{3.4}$$

It follows from Eq. (3.3) that the geodesic distance between $\hat{\mathbf{u}}$ and $\hat{\mathbf{u}}_0$ is $s=r$, as required by the rolling operation.

We shall be interested in the irreducible representations of SO(4). The six generators of SO(4) rotate the six distinct planes (o,x), (oy), (oz), (xy), (yz), and (xz) of a four-dimensional coordinate system. Here, x, y, and z denote directions in the physical flat space we are interested in, and o a direction $\hat{\mathbf{e}}_0$ orthogonal to these three. We shall use Greek indices to denote x, y, or z. The generators $L_{\mu\nu}$ rotate the tangent sphere, keeping the point of tangency and the axis $\hat{\mathbf{e}}_0$ fixed. These generators are related to conventional SO(3) angular momentum operators L_λ by $L_\lambda=\frac{1}{2}\epsilon_{\lambda\mu\nu}L_{\mu\nu}$.[17,18] The generators $L_{0\mu}$ roll the sphere in the direction $\hat{\boldsymbol{\mu}}$.

The so-called "diagonal" irreducible representations of SO(4) are obtained using the hyperspherical harmonics $Y_{n,m_am_b}(\hat{\mathbf{u}})$ as basis functions. The representation index n assumes the values $n=0,1,2,\ldots$, while the azimuthal quantum numbers m_a and m_b range in integer steps from $-n/2$ to $n/2$. These hyperspherical harmonics are themselves proportional to the Wigner *matrices* of SU(2) for the representation $l=n/2$.[17,18] The matrix elements of the generators of the nth representation of SO(4) can be expressed using the homomorphism between SO(4) and SU(2)×SU(2). We have[41]

$$L_{0\mu}=A_\mu+B_\mu^T \ , \tag{3.5a}$$

$$L_\mu=A_\mu-B_\mu^T \ , \tag{3.5b}$$

where the matrices A_μ and B_μ are generators of two independent, $l=n/2$ representations of SU(2). The matrix B_μ^T is the transpose of B_μ. The matrix A_μ acts only on the m_a index of Y_{n,m_am_b} while B_μ acts only on the m_b index. It is easy to verify that this parametrization satisfies the SO(4) commutation relations.[41]

We now check that the generators L_μ do indeed rotate the sphere about its point of tangency. Consider the action of the operator $\exp(-i\theta_\mu L_\mu)$ on the hyperspherical harmonic $Y_{n,m_am_b}(u)$, which we shall write, suppressing the azimuthal indices, as $Y_n(u)$. We shall show that the vector $\boldsymbol{\theta}$ parametrizes a rotation of θ about the $\hat{\boldsymbol{\theta}}$ axis. We have

$$\begin{aligned} \exp(-iL_\mu\theta^\mu)Y_n(u)&=e^{-\boldsymbol{\theta}\cdot(\mathbf{A}-\mathbf{B}^T)}Y_n(u) \\ &=e^{-i\boldsymbol{\theta}\cdot\mathbf{A}}Y_n(u)e^{+i\boldsymbol{\theta}\cdot\mathbf{B}} \\ &=Y_n(e^{-i\boldsymbol{\theta}\cdot\sigma/2}ue^{+i\boldsymbol{\theta}\cdot\sigma/2}) \ . \end{aligned} \tag{3.6}$$

In the last step, we have used the fact that $Y_n(u)$ is a Wigner matrix and the group property of the SU(2) Wigner matrices. Upon writing u in its SU(2) matrix form $u=w+i\mathbf{r}\cdot\sigma$, it is easily shown using the properties of the Pauli matrices that

$$\exp(-iL_\mu\theta_\mu)Y_n(u)=Y_n(w+i(\underset{\sim}{R}_{\boldsymbol{\theta}}\mathbf{r})\cdot\sigma) \ , \tag{3.7}$$

where $\underset{\sim}{R}_{\boldsymbol{\theta}}$ is a 3×3 rotation matrix which rotates $\mathbf{r}$ an amount θ about the axis $\hat{\boldsymbol{\theta}}$. The operator L_μ does indeed rotate the spacelike coordinates of u, leaving the coordinate w unchanged. Similar manipulations can be used to show that

$$\begin{aligned} \exp(-iL_{0\mu}\omega_\mu)Y_n(u)&=e^{-i\boldsymbol{\omega}\cdot\mathbf{A}}Y_n(u)e^{-i\boldsymbol{\omega}\cdot\mathbf{B}} \\ &=Y_n(u') \ , \end{aligned} \tag{3.8a}$$

where the components of u' are obtained from the components of u by rotating the plane spanned by $\hat{\mathbf{e}}_o$ and $\hat{\boldsymbol{\omega}}$ an amount ω. This relationship can be expressed in terms of SU(2) matrices by

$$u'=e^{-i\boldsymbol{\omega}\cdot\sigma/2}ue^{-i\boldsymbol{\omega}\cdot\sigma/2} \ . \tag{3.8b}$$

It is the same transformation as would be effected by rolling the tangent sphere a distance $s=\omega\kappa^{-1}$ in the direction $\hat{\boldsymbol{\omega}}$. Thus, the generator $L_{0\mu}$ produces the curved space analog of a "translation" in the μ direction.

Just as in Sec. II, we imagine projecting the particle density at $\mathbf{r}$ in flat space onto S^3, and expanding the resulting density $\rho_{\mathbf{r}}(\hat{\mathbf{u}})$ in the hyperspherical harmonics. If we denote the resulting Fourier coefficients by $Q_{n,m_am_b}(\mathbf{r})$, they are given by[24]

$$Q_{n,m_am_b}(\mathbf{r})=\int_{\Delta v'}\rho_{\mathbf{r}}(\hat{\mathbf{u}})Y_{n,m_am_b}(\hat{\mathbf{u}})d\Omega_{\hat{\mathbf{u}}} \ , \tag{3.9a}$$

where the integration volume $\Delta v'$ on the sphere has a length scale several times the spacing between defects. We can now define a density $\rho(\mathbf{r},\hat{\mathbf{u}})$ by

$$\rho(\mathbf{r},\hat{\mathbf{u}})\equiv\sum_{n,m_am_b}Q^*_{n,m_am_b}(\mathbf{r})Y_{n,m_am_b}(u) \ , \tag{3.9b}$$

where the physical density at the point $\mathbf{r}$ is given by $\rho(\mathbf{r},\hat{\mathbf{u}}_o)$, $\hat{\mathbf{u}}_o=(-1,0,0,0)$. The density at the point $\mathbf{r}+\boldsymbol{\delta}$ will be the same as the density obtained by rolling the sphere from the point $\mathbf{r}$ if

$$\rho(\mathbf{r}+\boldsymbol{\delta},\hat{\mathbf{u}})=\rho(\mathbf{r},\hat{\mathbf{u}}') \ , \tag{3.10a}$$

where $\hat{\mathbf{u}}'$ is related to $\hat{\mathbf{u}}$ by rolling in the $\boldsymbol{\delta}$ direction. Writing $\hat{\mathbf{u}}$ and $\hat{\mathbf{u}}'$ as SU(2) matrices, we have, using Eq. (3.8b),

$$u' = e^{-i\delta\cdot\sigma/2} u e^{-i\delta\cdot\sigma/2}$$
$$\approx (1+\tfrac{1}{2}i\delta\cdot\sigma)u(1+\tfrac{1}{2}i\delta\cdot\sigma) . \quad (3.10b)$$

Using Eq. (3.9b) and requiring that (3.10b) be satisfied to lowest order in δ gives us a condition on the $Q_{n,m_a m_b}(\mathbf{r})$, namely

$$\partial_\mu \mathbf{Q}_n = i\kappa L_{0\mu}^{(n)} \mathbf{Q}_n , \quad (3.11)$$

where $L_{0\mu}^{(n)}$ is a generator for the nth representation of SO(4). For notational convenience we have written $Q_{n,m_a m_b}$ as a $(n+1)^2$-dimensional "vector" $\mathbf{Q}_n$.

A Landau free energy which incorporates the physics embodied in Eq. (3.11) is[17]

$$F = \tfrac{1}{2}\sum_n [K_n \mid (\partial_\mu - i\kappa L_{0\mu}^{(n)})\mathbf{Q}_n \mid^2 + r_n \mid \mathbf{Q}_n \mid^2] + O(Q_n^2) . \quad (3.12)$$

The sum on n will be restricted to representations which have a component invariant under the symmetries of polytope $\{3,3,5\}$, i.e., $n = 12,20,34,30,32\ldots$. We neglect the unimportant uniform density mode at $n=0$. As we have already argued in the Introduction, the high density of defect lines that are present even in the supercooled liquid will force the order parameter to be small and make quadratic truncation of this free energy a plausible first approximation.

B. Diagonalization of the free energy

As in the preceding section, a first step in the further analysis of the density fluctuations is the diagonalization of this quadratic form. We first perform a Fourier transform and express the gradient part of the free energy in Fourier space:

$$\mathbf{Q}_n^*(\mathbf{k})[k^2 - 2\kappa\mathbf{k}\cdot(\mathbf{A}+\mathbf{B}^T) + \kappa^2(\mathbf{A}+\mathbf{B}^T)^2]\mathbf{Q}_n(\mathbf{k}) . \quad (3.13)$$

Now let $\underset{\sim}{R}$ be a rotation which rotates $\mathbf{k}$ into the z direction,

$$R_{ij}k_j = k\delta_{iz} . \quad (3.14a)$$

If $(\theta_{\hat{\mathbf{k}}}, \phi_{\hat{\mathbf{k}}})$ are the spherical polar coordinates of $\hat{\mathbf{k}}$, a convenient choice for $\underset{\sim}{R}$ is a rotation about the z axis by an angle $-\phi_k$ followed by a rotation of $-\theta_k$ about the y axis. The $l = n/2$ Wigner matrix corresponding to $\underset{\sim}{R}$ is

$$D_{m_a m_b}^{n/2}(\underset{\sim}{R}) = d_{m_a m_b}^{n/2}(-\theta_k) e^{i m_b \phi_k} , \quad (3.14b)$$

where the $d_{m_a m_b}^{n/2}$ are the reduced rotation matrices.[39] We now recall the property of the D matrices that

$$D(\underset{\sim}{R}^{-1}) L_i D(\underset{\sim}{R}) = R_{ij} L_j , \quad (3.14c)$$

where L_i are matrix generators of SU(2). Inserting the unit matrix in the form $D^{-1}D$ and using (3.14c), the gradient part of the free energy can be transformed into

$$\mathbf{C}_n^*(k)[k^2 - 2\kappa k(A_z + B_z^T) + \kappa^2(\mathbf{A}+\mathbf{B}^T)^2]\mathbf{C}_n(k) , \quad (3.15)$$

where $Q_{n,m_a m_b}$ is related to the $C_{n,m_a m_b}$ by (summation convention implied)

$$Q_{n,m_a m_b} = D_{m_a \bar{m}_a}^n (\underset{\sim}{R}^{-1}) C_{n,\bar{m}_a \bar{m}_b} D_{\bar{m}_b m_b}^n (\underset{\sim}{R}) , \quad (3.16)$$

and we have used the decomposition (3.5a). As in the preceding subsection, we define $\beta = k/\kappa$. It is easy to check that $C_{n,m_a m_b}$ behaves under the action of $\mathbf{A}$ and $\mathbf{B}$ like the composite angular momentum kets $|\, n/2\ m_a, n/2\ m_b \rangle$, where m_a and m_b are eigenvalues of A_z and B_z. It follows that to diagonalize the gradient part of the free energy we must diagonalize the $(n+1)^2 \times (n+1)^2$ matrix,

$$\Xi(\beta) \equiv \beta^2 - 2\beta(m_a + m_b) + n\left[\frac{n}{2}+1\right] + 2m_a m_b + A_+ B_+ + A_- B_- , \quad (3.17)$$

where $A_\pm$ and $B_\pm$ are standard quantum-mechanical raising and lowering operators.[39] The first four terms are diagonal in the m_a, m_b basis, while the last two terms are off diagonal. An important property of the off-diagonal terms is that they do not mix states with different values of M, where M is given by

$$M = m_a - m_b . \quad (3.18)$$

This is related to the fact that the quantity

$$\mathcal{M} = \hat{\mathbf{k}}\cdot(\mathbf{A} - \mathbf{B}^T) \quad (3.19)$$

commutes with original free energy (3.13). It follows that the quadratic form breaks into $(n - |M| + 1)$-dimensional subspaces indexed by the value of M.

The eigenvalues can be determined for large β by straightforward perturbation theory applied to the quadratic form (3.17). To order $1/\beta$ the eigenvalues of Ξ are

$$\lambda_{m_a m_b}^{(\beta)} = \beta^2 - 2(m_a+m_b)\beta + n\left[\frac{n}{2}+1\right] + 2m_a m_b - \frac{\left[\frac{n}{2}+m_a+1\right]\left[\frac{n}{2}+m_b+1\right]\left[\frac{n}{2}-m_a\right]\left[\frac{n}{2}-m_b\right]}{2m_a+2m_b+2-4\beta}$$
$$+ \frac{\left[\frac{n}{2}+m_a\right]\left[\frac{n}{2}+m_b\right]\left[\frac{n}{2}-m_a+1\right]\left[\frac{n}{2}-m_b+1\right]}{2m_a+2m_b-4\beta-2} . \quad (3.20)$$

This expression has a minimum as a function of β. The smallest eigenvalue occurs when $\beta \approx n$ for $m_a = m_b = n/2$ into the $M=0$ subspace and equals

$$\lambda_{\min}(n) \approx \frac{n(n+2)}{2(n+1)} . \tag{3.21}$$

The eigenvalues can also be determined for small values of β. We now have to return to the expression (3.13). The angular momentum generator B_μ^T is equivalent to a generator $-C_\mu$ by a simple unitary transformation given by

$$| m_a m_c \rangle = (-1)^{m_b} | m_a - m_b \rangle .$$

Here C_μ is a generator of SU(2) and satisfies the usual SU(2) commutation relations. In terms of the generators A_μ and C_μ, the matrix Ξ can be shown to be equivalent to

$$\Xi(\beta) = \beta^2 - 2\beta(A_z - C_z) + n\left[\frac{n}{2}+1\right] - 2\mathbf{A}\cdot\mathbf{C} . \tag{3.22}$$

This matrix, expressed in terms of the m_a, m_c basis, is mathematically the same as the Hamiltonian for two spin-$(n/2)$ particles in a staggered magnitude field, interacting via a Heisenberg exchange interaction. It is clear that the β-independent terms will be diagonal in a basis in which A_z, C_z, $A_z + C_z$, and $J^2 = (A+C)^2$ are diagonal. This basis is related to the m_a, m_c basis via a unitary transformation using standard quantum-mechanical Clebsch-Gordan coefficients.[39] The states in this basis are labeled by indices J, M with $0 \le J \le n$ and $-J \le M \le J$. The eigenvalues up to second order in n can now be determined using the standard properties of the Clebsch-Gordan coefficients and the Wigner-Eckart theorem. The J, M eigenvalue is

$$\lambda_{J,M}(\beta) = n(n+2) - J(J+1) + \beta^2 - 2\beta^2 \left[\frac{(J^2-M^2)[(n+1)^2-J^2]}{J(4J^2-1)} - \frac{[(J+1)^2-M^2][(n+1)^2-(J+1)^2]}{(J+1)[4(J+1)^2-1]} \right] . \tag{3.23}$$

The eigenvalues decrease quadratically with β and there is no minimum in sight.

By exploiting the angular momentum decomposition described above, it is straightforward to diagonalize the quadratic form numerically on the computer. The numerical computation is greatly aided by the fact that the different M subspaces do not mix. The result of numerically determining the lowest three eigenvalues in each M subspace for $n=12$ as a function of β is shown in Fig. 6. The eigenvalues in the $+M$ and $-M$ subspaces are degenerate. The perturbative estimates for the value and position of the minimum eigenvalue are consistent with the numerical calculation. As in the two-dimensional case, the fact that these eigenvalues are always positive is due to the frustration embodied in the gradient term.

Now let $e^{M,i}_{n,m_a m_b}$ be the exact orthonormal ith eigenvector in the M subspace and $\lambda^n_{M,i}$ be the corresponding eigenvalue. The eigenvalues are ordered such that $\lambda^n_{M,i}$ is a monotonically increasing function of i. Note that both the eigenvector and the eigenvalues are independent of the direction of $\mathbf{k}$. We can now expand both the free energy and the order parameter in terms of these eigenvectors. We get

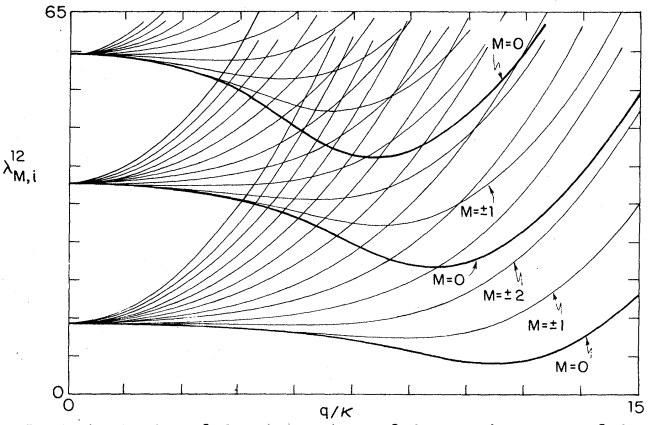

FIG. 6. A plot of the eigenvalues of the gradient part of the quadratic free energy describing icosahedral ordering in three dimensions. The eigenvalues shown are the three lowest eigenvalues for each M subspace of the $n=12$ representation. The eigenvalues belonging to the $M=0$ subspace are shown as heavy solid lines.

$$Q_{n,m_a m_b}(\mathbf{k}) = \sum_{M=-n}^{n} \sum_{i=1}^{n-|M|+1} \alpha^n_{M,i}(\mathbf{k}) D^{n/2}_{m_a \bar{m}_a}(R^{-1}) \times e^{m,i}_{n,\bar{m}_a \bar{m}_b}(k) D^{n/2}_{\bar{m}_b m_b}(R) , \tag{3.24a}$$

$$F = \tfrac{1}{2} \sum_{k,M,i,n} | \alpha^n_{m,i}(\mathbf{k}) |^2 [K_n \lambda^n_{m,i}(k) + r_n] , \tag{3.24b}$$

where $\alpha^n_{M,i}$ is a number parametrizing the strength of the ith eigenmode. The condition that the density be real gives us the constraints

$$Q_{n,m_a m_b}(\mathbf{k}) = (-1)^{m_a+m_b} Q^*_{n,-m_a-m_b}(-\mathbf{k}) . \tag{3.25a}$$

Using Eq. (3.24a) and the properties of the Wigner D matrices, this relationship can be shown to be equivalent to

$$\alpha^n_{M,i}(\mathbf{k}) = (-1)^M \alpha^{n*}_{M,i}(-\mathbf{k}) . \tag{3.25b}$$

Using the expressions (3.24) and (3.8) and the group of properties of the Wigner matrices, we obtain

$$\rho(\mathbf{k},\hat{\mathbf{u}}) = \sum \alpha^{n*}_{M,i}(\mathbf{k}) e^{M,i}_{n,m_a m_b}(k) Y_{n,m_a m_b}(R^{-1}\hat{\mathbf{u}}R) , \tag{3.26}$$

where

$$M = m_a - m_b . \tag{3.27}$$

The physical density is the density on the south pole of the sphere: $\hat{\mathbf{u}} = \hat{\mathbf{u}}_o$. Using the expression (3.26) above, and the fact that

$$Y_{n,m_a m_b}(-1)=(-1)^n\left[\frac{n+1}{2\pi^2}\right]^{1/2}\delta_{m_a m_b}\ ,$$

the physical density can be shown to be

$$\rho(\mathbf{k})=\sum_{n,i,m}(-1)^n\left[\frac{n+1}{2\pi^2}\right]^{1/2}\alpha^{n*}_{0,i}(\mathbf{k})e^{0,i}_{n,mm}\ . \tag{3.28}$$

We can understand the position of the minimum eigenvalue in Fig. 6 by directly rolling S^3. Let the system have density fluctuations only in this eigenmode for $n=12$. The physical density in a direction parallel to $\mathbf{k}$ is given by

$$\rho(r)=\sum_m\left[\frac{13}{2\pi^2}\right]^{1/2}e^{0,1}_{12,mm}(k_{\min})\cos(k_{\min}r)\ . \tag{3.29}$$

Now begin at the origin and roll S^3 in the direction parallel to $\mathbf{k}$. Using the expressions (3.26) and (3.4) the density deposited by S^3 at a distance r from the origin is

$$\rho(r)=\sum_m e^{0,1}_{12,mm}(k_{\min})\mathrm{Re}Y_{12,mm}[\cos(\kappa r)+i\sigma_z\sin(\kappa r)]\ . \tag{3.30}$$

The two densities (3.29) and (3.30) are plotted in Fig. 7(a). We can perform a similar exercise in a direction perpendicular to $\mathbf{k}$. The two densities in this case are

$$\rho(r)=\sum_m\left[\frac{13}{2\pi^2}\right]^{1/2}e^{0,1}_{12,mm}(k_{\min})\ \text{(flat space)}$$
$$\rho(r)=\sum_m e^{0,1}_{12,mm}(k_{\min})Y_{12,mm}[\cos(\kappa r)+i\sigma_x\sin(\kappa r)] \tag{3.31}$$
$$\text{(unrolled from } S^3)\ ,$$

and are plotted in Fig. 7(b). The density rolled from the sphere is quite close to the physical density. The free energy is designed to minimize the square of the difference of these two densities, averaged over all directions.

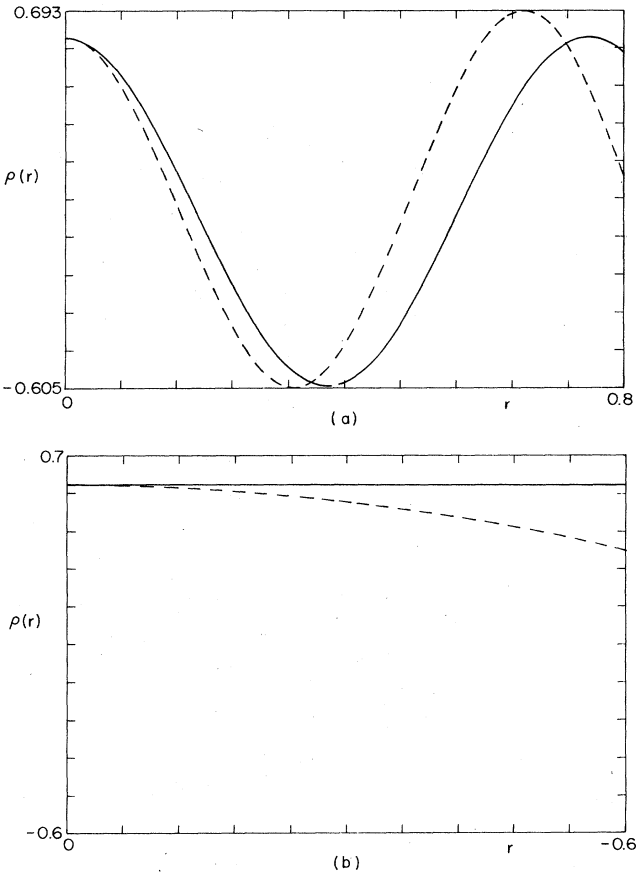

FIG. 7. Comparison between the density fluctuations of a given wave vector in flat space and those obtained by rolling the sphere. The sphere is constrained to have density fluctuations only in the mode with the minimum eigenvalue for $n=12$. The dotted lines represent the density rolled from the sphere, while the solid lines represent the density in flat space. Panel (a) exhibits the comparison in a direction parallel to the wave vector, while panel (b) shows the comparison perpendicular to the wave vector.

C. Structure factor of metallic glasses

Using the Gaussian free energy introduced in the preceding subsection, we can calculate the density-density correlation function of a metallic glass. As argued in the Introduction, truncation of the Ginzburg-Landau expansion at the quadratic order is reasonable because the large density of defects will force the order parameter to be small upon coarse graining. From Eq. (3.28) for the physical density in flat space and the free-energy density (3.24), we obtain

$$S(k)=\langle\rho(\mathbf{k})\rho(-\mathbf{k})\rangle$$
$$=\sum_{n=12,20,24,\ldots}\frac{n+1}{2\pi^2}\frac{k_BT}{K_n\lambda^n_{0,i}(k)+r_n}\left|\sum_m e^i_{n,mm}(k)\right|^2\ . \tag{3.32}$$

Note that because the physical density depends only upon the diagonal elements of $Q_{n,m_a m_b}$, it couples only to the $M=0$ subspace. In the preceding subsection we have already described a perturbative evaluation of the eigenvalues $\lambda^n_{M,i}$. We now turn to a description of the evaluation of the factor in the numerator:

$$\left|\sum_m e^{0,i}_{n,mm}(k)\right|^2\ .$$

As k tends to ∞, the quadratic form (3.17) becomes diagonal in the m_a,m_b basis. So we clearly have

$$\lim_{k\to\infty}\sum_m e^{0,i}_{n,mm}(k)=1\ . \tag{3.33}$$

As k tends to 0, the quadratic form is diagonal in the J,M basis introduced in the section following Eq. (3.22). It follows that

$$\lim_{k\to 0}e^{0,i}_{n,mm}(k)=\begin{bmatrix}n/2 & n/2 & J\\ -m & m & 0\end{bmatrix}(-1)^m\sqrt{2J+1}\ , \tag{3.34}$$

with $J=n-i+1$. The symbol on the right-hand side of the equation above is the usual 3-j symbol of the group

SU(2). Using well-known properties of the 3-j symbol, we may deduce that

$$\lim_{k\to 0}\sum_m e^{0,i}_{n,mm}(k)=(-1)^{n/2}\sqrt{n+1}\,\delta_{J0}\ . \tag{3.35}$$

For intermediate values of k numerical calculations show that

$$\left|\sum_m e^{i}_{n,mm}(k)\right|^2$$

interpolates smoothly between its values at 0 and ∞.

From the expression (3.32), and the fact that $e^{0,i}_{n,mm}$ is a smooth function of k, we see that there is a peak in the structure factor for each representation of SO(4) which is nonvanishing on polytope $\{3,3,5\}$. The peak occurs at the position of the minimum eigenvalue in the $M=0$ subspace. The calculation as presented above is directly applicable to monatomic metallic glasses. While it has not yet been experimentally possible to make such substances by cooling the melt, one can make thin films of amorphous metals by vapor deposition onto a cold substrate. It is believed that essentially the same structure would result if one could cool the melt fast enough.[6] Figure 8(a) shows a fit of our results to the measurements of Leung and Wright on amorphous cobalt.[3] Two parameters, K_n/k_BT_g and r_n/k_BT_g, have been adjusted for each peak. The peak positions q_n, however, are completely determined by the theory once κ is known: we find that $q_{12}=11.25\kappa$, $q_{20}=19.20\kappa$, and $q_{24}=22.96\kappa$. The theoretical value of the ratio q_{20}/q_{12} is 1% higher than the experimental value of 1.69, while the ratio q_{24}/q_{12} exceeds the experimental value 1.97 by 3.5%. The $n=30$ and $n=32$ peaks are quite close to each other and appear as a single peak in the experiment. The fits determine a set of masses $r_{12},r_{20},r_{24},\ldots$ which are all negative, consistent with the physical picture discussed in the Introduction. Table II shows the values of K_n and r_n determined from the fit.

The value of κ for amorphous cobalt is determined by fitting the result $q_{12}=11.25\kappa$ to the position of the first peak. The particle spacing d on the polytope then follows from the relation $\kappa d=\pi/5$. We find that d is about 10% less than the position of the first peak in the flat-space radial distribution function, lying approximately at the point of inflection. The smaller value of d is to be expected, since the mapping from flat space onto the tangent sphere (see, e.g., Fig. 2) compresses distances.

The behavior of K_n and r_n with n is summarized in Table II. To determine the peak widths and intensities, we note that, to a good approximation, we can assume that each peak in the structure factor is given by the minimum in the eigenvalue $\lambda^n_{0,1}(q)$ for a given n. The eigenvalue $\lambda^n_{0,1}(q)$ has a quadratic minimum at q_n, and we see that the center of each peak is approximately a Lorentzian. The width of this Lorentzian W_n and the intensity of the peak I_n (this is the number multiplying a normalized Lorentzian) are therefore given by

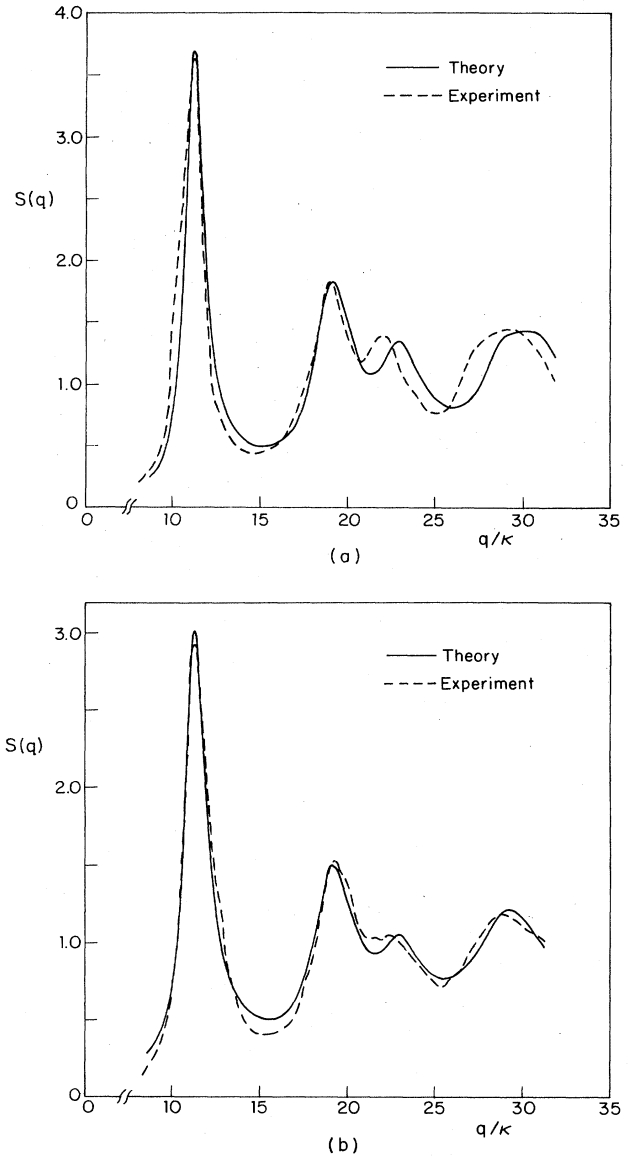

FIG. 8. (a) Comparison of the structure factor obtained by fitting the theoretical expression (3.32) to the experimental data on amorphous cobalt films obtained by Leung and Wright (Ref. 3). There are two adjustable parameters for each peak which determine its width and height. The peak positions, however, are a consequence of the theory. (b) Similar fit to the data of Lauriat (Ref. 4) for amorphous iron.

TABLE II. Landau parameters K_n/k_BT_g and r_n/k_BT_g and peak widths and intensities for amorphous cobalt (Ref. 3) as a function of n. All quantities are measured in units such that $\kappa=1$.

n	K_n/k_BT_g	r_n/k_BT_g	W_n	I_n
12	0.18	−0.89	0.63	6.9
20	0.16	−1.03	1.29	5.2
24	0.32	−2.37	1.36	2.8
30	0.30	−2.49	1.68	2.7
32	0.16	−1.23	2.21	4.0

$$W_n = \left[\frac{[K_n \lambda^n_{0,1}(q_n) + r_n]}{K_n \{ \frac{1}{2} [d^2 \lambda^n_{0,i}(q)/dq^2] \}_{q_n}} \right]^{1/2} , \tag{3.36a}$$

$$I_n = \frac{n+1}{2\pi} \left| \sum_m e^{0,i}_{n,mm}(q_n) \right|^2 \frac{k_B T}{([K_n \lambda^n_{0,1}(q_n) + r_n] K_n \{ \frac{1}{2} [d^2 \lambda^n_{0,1}(q)/dq^2] \}_{q_n})^{1/2}} . \tag{3.36b}$$

The values of W_n and I_n are tabulated in Table II. Examining this table we observe a uniform trend in increasing peak width as we move to higher n. The peak intensity decreases with n for the first four peaks. The increase in peak intensity with the $n=32$ peak is probably not real as the fitting parameters for the $n=30$ and 32 peaks are not reliable.

We have also performed a fit to experiments of Lauriat[4] on vapor-deposited amorphous iron. Figure 8(b) shows a comparison between the experimental data and the best theoretical fit. The ratio of the peak positions are a direct consequence of theory and a glance at Table III shows that the agreement between theory and experiment is good. Table III also contains data obtained from computer simulations of supercooled Lennard-Jones liquid.[7] This data serves as a direct check of the applicability of the theory to bulk systems.

Thus far all of the metallic glasses which have been made in the bulk by spin-cooling the melt have two or more components. Such substances can be incorporated into the theory above in the limit when most of the metallic glass is made up of one component. The effect of the other components can be represented by an additional luctuating impurity concentration $c(\mathbf{r})$. The $c(\mathbf{r})$ will tend to destroy the local icosahedral ordering and we therefore expect it to broaden the peaks in the structure factor. The simplest way in which $c(\mathbf{r})$ can couple to the order parameter is via the replacement

$$F \to F + \int d^3r \left[\sum_n \gamma_n c \, | \, \mathbf{Q}_n \, |^2 + \frac{1}{2} \frac{c^2}{\chi} - c\Delta \right] , \tag{3.37a}$$

where χ is the concentration susceptibility, the γ_n are coupling constants, and Δ is an impurity chemical potential. γ_n and Δ must both be positive if an excess impurity concentration destroys the local icosahedral ordering. The impurity concentration can also change the local value of κ, but this effect will be small if the system is mostly one component. It is straightforward to integrate out the impurity concentration in expression (3.36). Its only effect on the $\mathbf{Q}_n$ to lowest order in γ_n is to replace

$$r_n \to r_n + \tfrac{1}{2} \gamma_n \Delta\chi . \tag{3.37b}$$

This replacement simply leads to a broadening of the peaks in the structure factor without significantly changing their positions. This seems to be what is observed experimentally.[1]

D. Effect of nonlinearities

We have argued that a Gaussian truncation of the free energy is a plausible first approximation to describing icosahedral ordering in supercooled liquids. In this section we shall attempt to estimate the effect of nonlinearities. In particular, we shall be interested in how the third-order terms in the free energy shift the positions of the peaks q_{12}, q_{20}, and q_{24} in the structure factor. We shall try to understand, in particular, the small discrepancy between theory and experiment in the $n=24$ peak (see Table III). We shall focus on the data tabulated in Ref. 3 [see Fig. 8(a)].

Following Ref. 17, we deduce the form of the third-order term by simply writing down the most general terms consistent with the symmetries of polytope $\{3,3,5\}$,

$$F = \tfrac{1}{2} \sum_n [K_n \, | \, (\partial_\mu - i\kappa \mathbf{L}^{(n)}_{0\mu}) \mathbf{Q}_n \, |^2 + r_n \, | \, \mathbf{Q}_n \, |^2] + \sum_{\substack{n_1,n_2,n_3 \\ m_1,m_2,m_3 \\ \bar{m}_1,\bar{m}_2,\bar{m}_3}} w_{n_1 n_2 n_3} Q^{n_1}_{m_1 \bar{m}_1} Q^{n_2}_{m_2 \bar{m}_2} Q^{n_3}_{m_3 \bar{m}_3} \begin{bmatrix} n_1 & n_2 & n_3 \\ m_1 & m_2 & m_3 \end{bmatrix} \begin{bmatrix} n_1 & n_2 & n_3 \\ \bar{m}_1 & \bar{m}_2 & \bar{m}_3 \end{bmatrix} , \tag{3.38}$$

where the parentheses on the right-hand side denote the usual Wigner 3-j symbols of SU(2). Notice that we have introduced a large number of unknowns $w_{n_1 n_2 n_3}$ as the coefficients of the third-order terms. This shall not prove to be a disadvantage because we shall argue that the effect of the nonlinearities on the structure factor at a given q is dominated by a single third-order term. We shall examine the variation of this term for wave vectors near the peak position. In this way we shall be able to estimate the rela-

TABLE III. Relative peak positions in the structure factor.

	Theory	Amorphous cobalt[a]	Amorphous iron[b]	Computer simulations[c]
q_{20}/q_{12}	1.71	1.69	1.72	1.7
q_{24}/q_{12}	2.04	1.97	1.99	2.0

[a]Reference 3.
[b]Reference 4.
[c]Reference 5.

tive size of the shifts of the peak positions and find that the $n=24$ peak is moved closer to the experimentally observed position, with much smaller shifts in the $n=12$ and 20 peaks.

The gist of the argument is as follows. The dominant contribution of the third-order terms can be represented by the bubble graph of Fig. 9. There are three factors which determine the magnitude of a graph: (1) the vertex coefficients, which are slowly varying functions of q; (2) the magnitude of the propagators, which tells us to concentrate upon modes with $M=0$, $i=1$, and q near q_{12}; (3) the phase-space factor. It is the phase-space factor which gives the most rapid variation in the self-energy. In particular, it gives a sharp maximum in self-energy near $2q_{12}$, pulling the position of the $n=24$ peak towards $2q_{12}$.

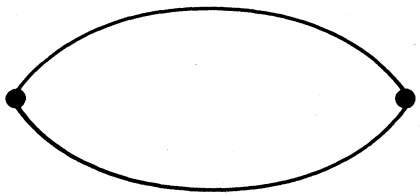

FIG. 9. Lowest-order bubble graph for the self-energy.

We begin by writing the free-energy density (3.38) in terms of variables which diagonalize the quadratic form: $\alpha^n_{M,i}(\mathbf{q})$. In these variables the free energy is a sum in Fourier space of terms $F_{\mathbf{q}}$, where

$$F_{\mathbf{q}}=\tfrac{1}{2}\sum_{n,M,i}[K_n\lambda^n_{M,i}(q)+r_n]\,|\,\alpha^n_{M,i}(\mathbf{q})\,|^2\sum_{\substack{\mathbf{q}_1,\mathbf{q}_2,\mathbf{q}_3\\(\mathbf{q}_1+\mathbf{q}_2+\mathbf{q}=0)\\ n_1,n_2,n_3\\ M_1,M_2,M_3\\ i_1,i_2,i_3}}\frac{w_{n_1n_2n_3}}{\sqrt{V}}\begin{Bmatrix} n_1 & n_2 & n_3\\ M_1 & M_2 & M_3\\ i_1 & i_2 & i_3\\ \mathbf{q}_1 & \mathbf{q}_2 & \mathbf{q}_3\end{Bmatrix}\alpha^{n_1}_{M_1,i_1}(\mathbf{q}_1)\alpha^{n_2}_{M_2,i_2}(\mathbf{q}_2)\alpha^{n_3}_{M_3,i_3}(\mathbf{q})\ . \tag{3.39}$$

We have introduced a coupling coefficient which has the following expansion in terms of the 3-j symbols, the D matrices, and the normalized eigenvectors of the quadratic form

$$\begin{Bmatrix} n_1 & n_2 & n_3\\ M_1 & M_2 & M_3\\ i_1 & i_2 & i_3\\ \mathbf{q}_1 & \mathbf{q}_2 & \mathbf{q}_3\end{Bmatrix}=\begin{bmatrix} n_1 & n_2 & n_3\\ m_1 & m_2 & m_3\end{bmatrix}\begin{bmatrix} n_1 & n_2 & n_3\\ \bar{m}_1 & \bar{m}_2 & \bar{m}_3\end{bmatrix}D^{n_1/2}_{m_1m_1'}(\underset{\sim}{R}_{q_1}^{-1})e^{M_1i_1}_{n_1m_1'\bar{m}_1'}(q_1)D^{n_1/2}_{\bar{m}_1'\bar{m}_1}(\underset{\sim}{R}_{q_1})$$

$$\times D^{n_2/2}_{m_2m_2'}(\underset{\sim}{R}_{q_2}^{-1})e^{M_2i_2}_{n_2m_2'\bar{m}_2'}(q_2)D^{n_2/2}_{\bar{m}_2'\bar{m}_2}(\underset{\sim}{R}_{q_2})D^{n_3/2}_{m_3m_3'}(\underset{\sim}{R}_{q_3}^{-1})e^{M_3i_3}_{n_3m_3'\bar{m}_3'}(q_3)D^{n_3/2}_{\bar{m}_3'\bar{m}_3}(\underset{\sim}{R}_{q_3})\ . \tag{3.40}$$

It satisfies the equality

$$\begin{Bmatrix} n_1 & n_2 & n_3\\ M_1 & M_2 & M_3\\ i_1 & i_2 & i_3\\ \mathbf{q}_1 & \mathbf{q}_2 & \mathbf{q}_3\end{Bmatrix}=(-1)^{M_1+M_2+M_3}\begin{Bmatrix} n_1 & n_2 & n_3\\ +M_1 & +M_2 & +M_3\\ i_1 & i_2 & i_3\\ -\mathbf{q}_1 & -\mathbf{q}_2 & -\mathbf{q}_3\end{Bmatrix}^*\ . \tag{3.41}$$

We shall focus our attention upon the form of the α-α Green's function:

$$G_{n_1M_1i_1;n_2M_2i_2}(\mathbf{q})=\langle\alpha^{n_1}_{M_1i_1}(-\mathbf{q})\alpha^{n_2}_{M_2i_2}(\mathbf{q})\rangle\ . \tag{3.42}$$

The structure factor can be expressed as a sum over these Green's functions:

$$S(q)=\sum_{\substack{n_1,n_2\\ i_1,i_2}}\left[\frac{(n_1+1)(n_2+1)}{4\pi^4}\right]^{1/2}(-1)^{n_1+n_2}\left[\sum_m e^{0i_1}_{n_1mm}\right]^*\left[\sum_m e^{0i_2}_{n_2mm}\right]G_{n_10i_1;n_20i_2}(q)\ . \tag{3.43}$$

The effect of the nonlinearities can be expressed in a matrix self-energy $\Sigma(\mathbf{q})$ which changes the Green's functions in the manner

$$G^{-1}(q)=G_0^{-1}(q)-\Sigma(q)\ . \tag{3.44}$$

The bare Green's function G_0 is a diagonal matrix with its matrix elements being the eigenvalues of the quadratic form.

We now argue that the largest term in the self-energy at any wave vector $\mathbf{q}$ to second order in the w's is given by the graph shown in Fig. 9. The propagators in the graph lie at a wave vector within the first peak of the structure

factor. If a propagator belongs to the mode $\{n,M,i\}$, it contributes to the graph a factor which is k_BT times the reciprocal of $K_n\lambda^n_{M,i}(\mathbf{q})+r_n$. This factor will clearly be large for the modes dominating the maximum in $S(\mathbf{q})$. These modes belong to $M=0$, $i=1$ and lie at a wave vector near q_n corresponding to the minimum eigenvalue of the gradient term for the representation n. It is this same minimum eigenvalue which gave rise to peaks in the structure factor. It is clear therefore that as a first approximation we need only consider the effect of modes with $M=0$ and $i=1$ at wave vectors near the minimum eigenvalue. The size of the propagators for these modes will be roughly proportional to the size of the peak in the structure factor for the corresponding n.

From the argument above and Eqs. (3.43) and (3.44), it follows that the position of the peak belonging to the representation n will be sensitive to the magnitude of $\Sigma_{n01;n01}(q)$. A positive value of $\Sigma_{n01;n01}(q)$ will increase the height of the structure factor at that q. It is therefore necessary only to examine the behavior of $\Sigma_{n01;n01}(q)$ for q's which are near q_n. The maximum of $\Sigma_{n01;n01}(q)$ will give the position at which the peak in the structure factor would lie if it was solely determined by the third-order term. We expect the peak in the structure factor belonging to the representation n to lie somewhere between the minimum in $\lambda^n_{0,1}$ and the maximum in $\Sigma_{n01;n01}(q)$. The exact position will be determined by the magnitude of $w_{n,12,12}$.

We now estimate the position of the maximum of $\Sigma_{n01;n01}(q)$ by evaluating the graph in Fig. 9 with the propagators lying at q_{12}. As the $n=12$ peak in the structure factor is sharp this should give a reasonable estimate of the position of the maximum of $\Sigma_{n01;n01}(q)$. The phase space remaining after so constraining the propagators is a circle of radius $[q_{12}^2-(q/2)^2]^{1/2}$. Therefore we can obtain a good estimate of the position of the maximum of $\Sigma_{n01;n01}(q)$ by looking at the variation of

$$\Lambda_n(q)\equiv\left|\begin{Vmatrix} n & 12 & 12 \\ 0 & 0 & 0 \\ 1 & 1 & 1 \\ \mathbf{q} & \mathbf{q}_{12} & \mathbf{q}_{12} \end{Vmatrix}\right|^2 [q_{12}^2-(q/2)^2]^{1/2}\,. \qquad (3.45)$$

Figures 10(a), 10(b), and 10(c) show $\Lambda_n(q)$ plotted for $n=12$, $n=20$, and $n=24$, respectively. The ranges for the wave vector q are chosen to lie in a small interval around the respective q_n's. From Fig. 10(a) we note that the position of the maximum of $\Lambda_{12}(q)$ occurs very close to the experimental value. $\Lambda_{12}(q)$ also varies rather slowly across the peak. We therefore do not expect the cubic terms to have any significant effect on the $n=12$ peak. Figure 10(b) shows that $\Lambda_{20}(q)$ is also a slowly varying function of q. The experimental peak lies in between the quadratic prediction for the peak in the structure factor and the maximum in $\Lambda_{20}(q)$. This fact is consistent with the discussion above, indicating that nonlinearities could introduce a 1% shift in the position of q_{12}. From Fig. 10(c) we note that the vanishing of the phase space for the graph for $\Lambda_{24}(q)$ at $q=2q_{12}$ forces $\Lambda_{24}(q)$ to decrease to zero at $2q_{12}$ with a square-root cusp. This rapid variation

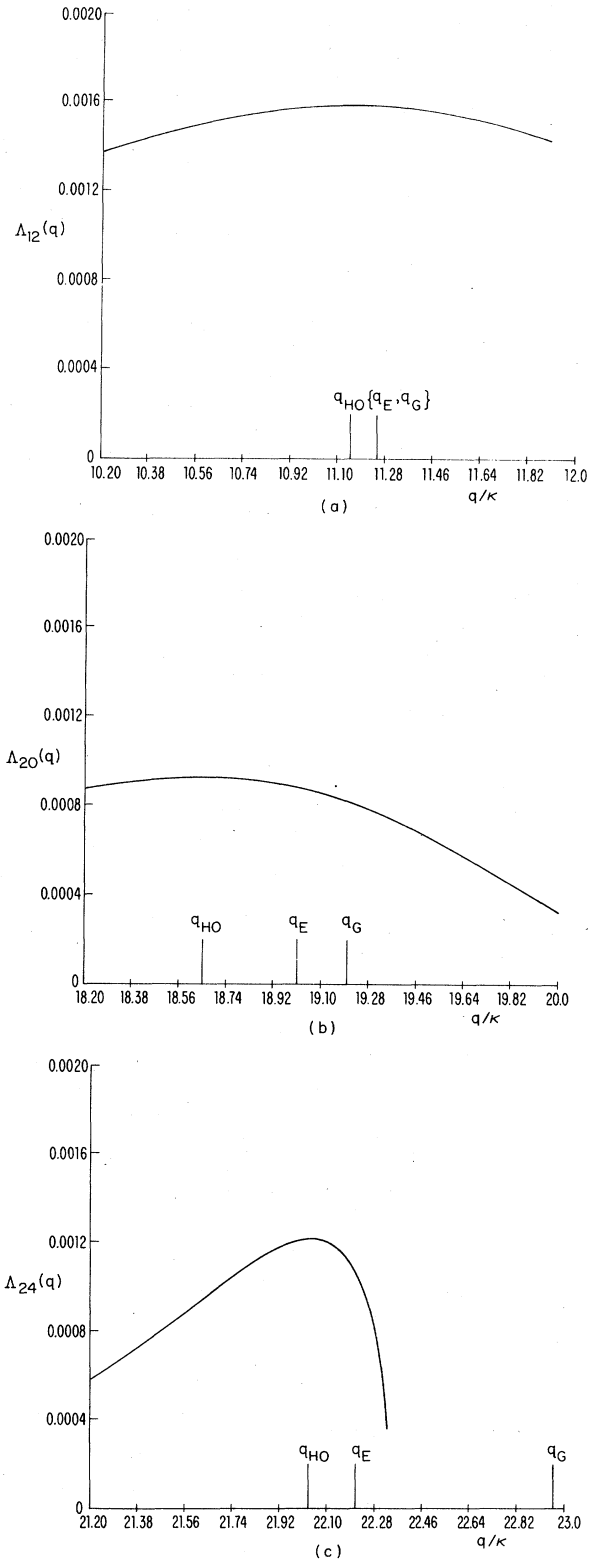

FIG. 10. These figures show plots of $\Lambda_n(q)$ for $n=12$, 20, and 24. The line at q_E marks the position of the peak in the experimental structure factor, that at q_G marks the theoretical prediction in the quadratic approximation and that at q_{H0} marks the position at which the effect of the cubic terms is at a maximum.

in the self-energy should have a pronounced effect upon q_{24}. The experimental position again lies in between the quadratic prediction for the peak in the structure factor and the maximum in $\Lambda_{24}(q)$. We have thus exhibited a mechanism by which it is possible to have a negligible shift in the peak position for $n=12$ and a much larger effect upon the $n=24$ peak than the $n=20$ peak.

We now make an order-of-magnitude estimate of the values of $\Sigma_{24,0,1;24,0,1}(q)$ and $w_{24,12,12}$ necessary to produce the necessary shift in the $n=24$ peak. The self-energy will shift the position of the maximum in the structure factor from the Gaussian prediction $q_G=q_{24}$ to the experimental position q_E if the magnitude of $\Sigma_{24,0,1;24,0,1}(q_E)$ is approximately

$$\begin{aligned}\Sigma_{24,0,1;24,0,1}(q_E)&\approx[K_{24}\lambda_{0,1}^{24}(q_E)+r_n]-[K_{24}\lambda_{0,1}^{24}(q_G)+r_n]\\&\approx 0.46-0.40\\&\approx 0.06\ .\end{aligned}\tag{3.46}$$

The parameter $w_{24,12,12}$ is a dimensionful parameter, so we need suitable units to judge its magnitude. A natural unit of length in this problem is κ^{-1}. In units where K_n and r_n are dimensionless, $w_{24,12,12}$ has units of $\kappa^{-3/2}$. In all our subsequent discussion, the value of $w_{24,12,12}$ will be expressed in these units. A simple way to implement these units is to perform all q-space integrals in units of κ.

To make an estimate of the value of $\Sigma_{24,0,1;24,0,1}(q_E)$ we need to perform the integral in q space of the graph in Fig. 9. We make a crude approximation by assuming that the integrand is significant only in a tube of radius $[q_{12}^2-(q/2)^2]^{1/2}$ with a cross-sectional area given by the square of the width of the first peak in the structure factor. This cutoff in cross-sectional area arises from the fact that the propagators in the graph are large only when they carry a momentum near q_{12}. In units of κ the width of this peak is approximately 3. So a rough estimate of the value of $\Sigma_{24,0,1;24,0,1}(q_E)$ is

$$\begin{aligned}\Sigma_{24,0,1;24,0,1}(q_E)&\approx(w_{24,12,12}^2)2\pi\Lambda_{24}(q_E)\frac{1}{(2\pi)^3}\frac{1}{[K_{12}\lambda_{0,1}^2(q_{12})+r_{12}]^2}(3)^2\\&\approx w_{24,12,12}^2(0.075)\ .\end{aligned}\tag{3.47}$$

Comparing this with Eq. (3.46) we see that the value of $w_{24,12,12}$ must be approximately 0.8 to shift the peak to the experimental position. This value of $w_{24,12,12}$ is of the same order of magnitude as the K_n's and the r_n's. However, when a value of $w_{24,12,12}$ in this range is coupled with the q-space integrals and the Clebsch-Gordan coefficients, under conditions in which these factors are largest, it yields a value of the self-energy correction to G^{-1} which is only 10% of the value of G_0^{-1}. [See Eq. (3.46).] As we have argued earlier, a self-energy correction of this magnitude has a pronounced effect upon the position of the $n=24$ peak and is ineffective in shifting the position of the $n=20$ and $n=12$ peaks.

Examining the effect of bubble graphs with the intermediate propagators lying at other q_n, we find no other vanishings of phase space near the first three peaks, implying that these graphs should not have a significant effect upon the peak positions. Furthermore, the overall magnitude of these graphs is smaller at least by a factor of 2 from the magnitude of the graphs in which both the propagators lie near q_{12}. This is because the size of the $n=12$ peak in the structure factor is at least a factor of 2 greater than the other peaks.

We have now shown that a Gaussian truncation of the free energy yields a self-consistent fit to the experimental data. The self-energy corrections to G^{-1} are at the most 10% of the value of G_0^{-1}. A self-energy correction of this magnitude has a pronounced effect upon the $n=24$ peak simply because of the accident that $q_{24}\approx 2q_{12}$. The effect of the self-energy upon the $n=12$ and $n=20$ peaks is much smaller.

ACKNOWLEDGMENTS

It is a pleasure to acknowledge useful conversations with E. Chason, B. I. Halperin, F. Spaepen, J. P. Straley, D. Turnbull, and M. Widom. This work was supported by the National Science Foundation, through the Harvard Materials Science Laboratory and through Grant No. DMR-82-07431.

APPENDIX A: THE FRANK-KASPER ALLOYS

In this appendix we will compare the short-range order in the Frank-Kasper alloys to the ordering in metallic glasses. The strong local icosahedral ordering in these alloys is broken up into a regular array of disclination lines. This is in contrast to metallic glasses where the degree of icosahedral ordering is smaller and the network of disclination lines is disordered. It is nevertheless instructive to compare the structure factor of a metallic glass and a Frank-Kasper phase with a very large unit cell, e.g., $Mg_{32}(Al,Zn)_{49}$. This particular Frank-Kasper phase[16] has a bcc lattice with a unit cell of 81 atoms. Within each unit cell this alloy starts out with three shells totaling 45 atoms placed in a way so that their mutual coordination is exactly the same as in polytope $\{3,3,5\}$. The remaining 36 atoms are placed in the outermost shell to make a structure with the shape of a bcc unit cell. To make a comparison between the structure factor of $Mg_{32}(Al,Zn)_{49}$ and a metallic glass, it is important to factor out the part of the structure factor which arises from the long-range bcc ordering in the crystal. This may be done most simply by calculating a spherical average of the form factor of a unit cell $F(q)$. We assume, for simplicity, that all atoms are identical, δ-function scatterers, and obtain

$$F(k)=\tfrac{1}{81}\sum_{i,j}\frac{\sin(kr_{ij})}{kr_{ij}}\ .\tag{A1}$$

The sum over i and j extends over all 81 atoms in the unit cell. The coordinates of the particles in a unit cell were

determined by allowing the system to relax in a nearest-neighbor Lennard-Jones pair potential. The initial coordinates were chosen to be consistent with the symmetries and coordination numbers of $Mg_{32}(Al,Zn)_{49}$. Figure 11 shows a comparison between the structure factor of amorphous cobalt films and the spherically averaged form factor of the $Mg_{32}(Al,Zn)_{49}$ structure. The value of κ for the form factor was chosen to make the first peaks coincide. Two points should be noted: (1) the peaks of the $Mg_{32}(Al,Zn)_{49}$ structure are broader than those of the metallic glass, presumably due to the constraints of bcc symmetry upon the third shell of atoms in the unit cell; (2) the gross structure of the first three peaks is similar in the two systems.

It is important, however, not to lose sight of the fact that the Frank-Kasper crystals are described by a low-temperature approach to icosahedral packing while metallic glasses are high-temperature realizations. We now examine whether the low-temperature fixed-length analysis of Appendix B can be related to the structure of the Frank-Kasper phases. There, we show that the two SU(2) groups present in the SO(4) symmetry of S^3 decouple in the fixed-length limit. The gradient term in the SU(2) free-energy density (B13) predicts a "twist" in the order parameter in all directions. Stated differently, in moving between two neighboring points, the order parameter tends to rotate about an axis joining the two points. This is very reminiscent of what happens in cholesteric liquid crystals. There the reference order parameter is a nearly uniaxial director which, because of an intrinsic chirality, tends to rotate between neighboring points. The one-Frank-constant approximation for the free-energy density of the cholesteric liquid crystal is

$$F=\tfrac{1}{2}K(\partial_i n_j-\kappa\epsilon_{ijk}n_k)^2 . \tag{A2}$$

This is simply the second term of the free-energy density (B13) written in the $l=1$ representation. An important difference is that the trace is over a uniaxial director which is not equivalent to an isotropic average. This propensity for inducing twists in all directions is the reason for the existence of the "blue" phases.[42] The blue phases are ordered networks of disclination lines. The defect-free regions tend to have a uniaxial director twisting in all directions.

In the case of interest the twists in the two SU(2) order parameters combine, as expected, to roll polytope $\{3,3,5\}$ between neighboring points. If polytope $\{3,3,5\}$ is rolled along any equator, the icosahedra centered at two neighboring points are found to be twisted relative to each other by an angle of $\pi/5$. To complete the picture of the Frank-Kasper phase it would be satisfying to identify this twist in the crystalline Frank-Kasper structures. In their analysis, Frank and Kasper[16] noted that the requirement of icosahedral coordination among atoms leads inevitably to approximately planar layers of atoms. A basic structure which appeared naturally when one tried to make a "primary" layer of defect-free atoms was the Kagome net (see Fig. 12). All the Frank-Kasper phases with trigonal symmetry—the Laves phase ($MgZn_2$, $MgCu_2$, $MgNi_2$, $CaZn_5$), the μ phase Fe_7W_6, and a host of other hypothetical structures proposed by Frank and Kasper—are made up of layers of Kagome nets alternating with layers of defect sites. By introducing "sequence faults" in the Kagome nets one can also obtain structures consistent with cubic symmetry: the σ phase, β-uranium, and $CuAl_2$ are examples of such structures. A Kagome net with "sequence faults" as occurring in the σ phase is shown in Fig. 13. Every atom on the Kagome nets is at the center of an icosahedron. The atoms lie along straight lines extending in three different directions. A remarkable property of these straight lines of atoms is that the icosahedra centered on them rotate from one atom to the next by an

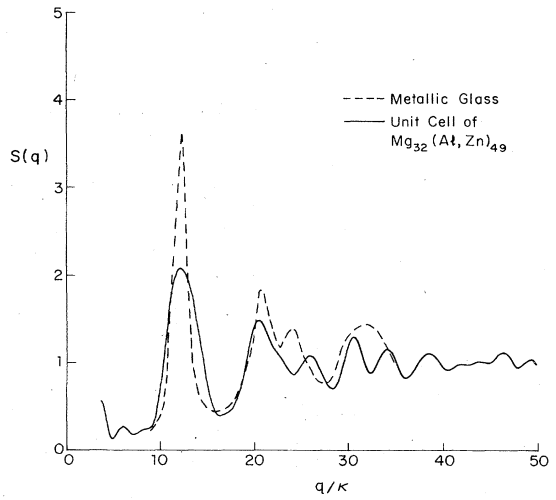

FIG. 11. Comparison between $S(q)$ of a metallic glass and of the Frank-Kasper phase $Mg_{32}(Al,Zn)_{49}$. The scale of the $S(q)$ of $Mg_{32}(Al,Zn)_{49}$ has been adjusted to make the first peaks coincide.

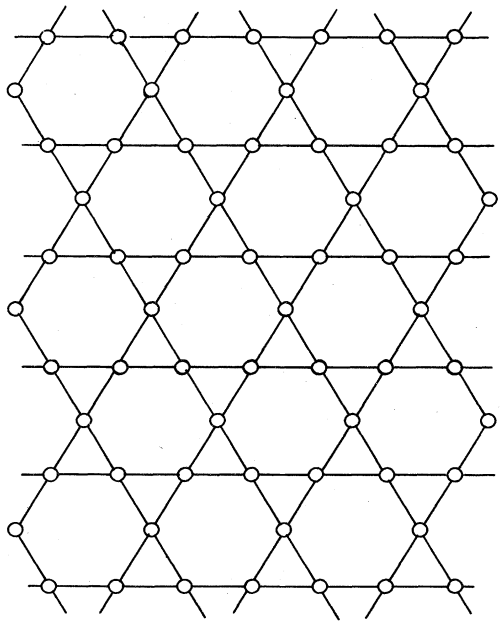

FIG. 12. A Kagome net of atoms.

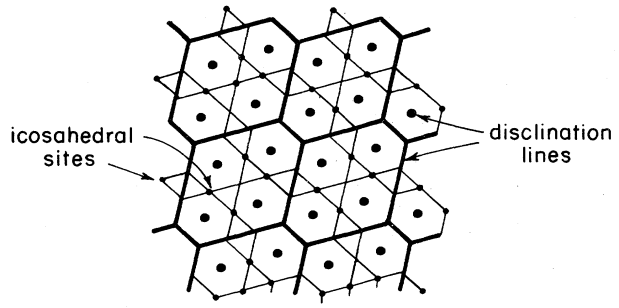

FIG. 13. A Kagome net with sequence faults as in the σ phase.

angle of $\pi/5$. This is remarkably similar to the twist along any equator of polytope $\{3,3,5\}$.

APPENDIX B: FIXED-LENGTH LIMIT

In this appendix we will present a synopsis of a low-temperature, fixed-length approach towards understanding the physics predicted by the free-energy density (1.3). By fixed length we mean that amplitude fluctuations are neglected except at the cores of defects, and the dominant fluctuations are simply rotations of a reference icosahedral order parameter. Such an approach will provide a good description of the order parameter at low temperatures in a configuration in which the cores of the defects are well separated. Because the defect density in the Frank-Kasper phases is large and the defect cores almost overlap, the fixed-length approach may be of limited use. Here, we (1) write down the form of the free energy after eliminating all degrees of freedom except for rotations of the icosahedral order parameter and an overall magnitude fluctuation near the cores of the defects: in this limit, theory is related to the continuum elastic approach of Sethna;[15] (2) we use the homomorphism between SO(4) and SU(2)⊗SU(2) to simplify considerably the form of the free-energy density; and (3) we evaluate the energy of a low-density configuration of parallel disclination lines. A Frank-Kasper phase has disclination lines running in several directions. Evaluation of the energy in such a situation is difficult even in the fixed-length limit. We will concentrate in this appendix upon the physics of icosahedral ordering in three dimensions. It is straightforward to extend the analysis of this appendix to analyze the low-temperature limit in the two-dimensional system with pentagonal ordering.

In a region of strong icosahedral ordering, the $n=12$ order parameter $Q_{12,m_a m_b}$ takes on the following value for a particular orientation of the coordinate axes:[17]

$$Q^0_{12,m_a m_b}=Q^0_{6,m_a}Q^0_{6,m_b}q\ , \tag{B1a}$$

where

$$Q^0_{6,m}=\tfrac{1}{5}(0,-\sqrt{7},0,0,0,0,\sqrt{11},0,0,0,0,\sqrt{7},0) \tag{B1b}$$

and q is a real number representing the magnitude of the order parameter. We will assume therefore that the order parameter only takes on values which are rotations of $Q^0_{12,m_a m_b}$. For simplicity we will concentrate on the $n=12$ representation, but as we shall show later, the results will be independent of the representation chosen. The amplitude q will be constant at most places but will go to zero at the cores of the defects.

We parametrize the order parameter as

$$Q_{12,m_a m_b}(\mathbf{r})=D^A_{m_a\bar{m}_a}(\mathbf{r})Q^0_{12,\bar{m}_a\bar{m}_b}(\mathbf{r})D^B_{\bar{m}_b m_b}(\mathbf{r})\ , \tag{B2}$$

where D^A and D^B are independent Wigner matrices belonging to the $l=6$ representation of SU(2). D^A and D^B together generate all possible rotations of SO(4). An important property of $Q^0_{6,m}$ is that

$$\begin{aligned} Q^{0*}_6 L_\mu Q^0_6&=\frac{1}{(2l+1)}\mathrm{Tr}(L_\mu)=0\ ,\\ Q^{0*}_6 L_\mu L_\nu Q^0_6&=\frac{1}{(2l+1)}\mathrm{Tr}(L_\mu L_\nu)=\tfrac{1}{3}l(l+1)\delta_{\mu\nu}\end{aligned} \tag{B3}$$

with $l=6$. Here L_μ is a matrix generator of SU(2) in the $l=6$ representation. The above property indicates that averages over $Q^0_{12,m_a m_b}$ are the same as averages over an isotropic state. This property can be shown to hold to up to products of four generators of SU(2).

We will now insert the ansatz (B2) into the free-energy density (1.3). An important property of the D matrices is that the expressions $D^{-1}\partial_\mu D$ and $D^{-1}L_\mu D$ belong to the Lie algebra SU(2). But we noted in (B3) that averages over the reference icosahedral parameter were equivalent to traces. So we may replace the $Q^0_{12,m_a m_b}$'s in the expression above by traces. We also note the properties

$$\mathrm{Tr}D^{-1}\partial_\mu D=0,\quad \mathrm{Tr}D^{-1}L_\mu D=0 \tag{B4}$$

because all the elements of the Lie algebra SU(2) are traceless. Using these properties, the free-energy density associated with Eq. (1.3) becomes

$$\mathcal{F}_{12}=\frac{1}{2(n+1)}K_n\mathrm{Tr}[(\partial_\mu q)^2-(D^{A^{-1}}\partial_\mu D^A-i\kappa D^{A^{-1}}A_\mu D^A)^2-(D^{B^{-1,T}}\partial_\mu D^{B^T}-i\kappa D^{B^{-1,T}}B^T_\mu D^{B^T})^2]+r_n q^2 \tag{B5}$$

with $n=12$. Two remarkable properties of the expression above should be noted. (1) We have used the homomorphism between SO(4) and SU(2)⊗SU(2) to show that the two SU(2) groups decouple in the fixed-length limit. After a simple unitary transformation, the free energy of the two groups in Eq. (B9) is the same up to an unimportant change in sign of κ. *Therefore from now on we will drop the second group from all our expressions, assuming that it has been treated in a manner similar to the first group.* (2) The expressions $D^{-1}\partial_\mu D$ and $D^{-1}L_\mu D$ depend only upon the properties of the SU(2) algebra and are independent of the representation of the D matrices and the L_μ. Expression (B5) is manifestly dependent only upon the commutation relations of SU(2). We use this independence upon representation, to work in the

simplest possible representation of SU(2): the $l=\frac{1}{2}$ representation in which the D matrices are 2×2 unitary matrices. Also note from (B4) that the trace over two or fewer matrices of SU(2) is independent of representation up to a change of scale. Let $\mathcal{U}$ denote a 2×2 unitary matrix. Then the free-energy density becomes

$$F=\frac{1}{2}K_n\left[(\partial_\mu q)^2-\frac{n(n+2)}{6}q^2\mathrm{Tr}\left[\mathcal{U}^\dagger\partial_\mu\mathcal{U}-\frac{i\kappa}{2}\mathcal{U}^\dagger\sigma_\mu\mathcal{U}\right]^2\right]+\frac{1}{2}r_nq^2\,, \tag{B6}$$

where the σ_μ are the Pauli matrices. This free-energy density is almost identical to the continuum elastic model of Sethna.[15] Sethna uses the vector representation of SO(4) and does not decompose SO(4) into its component SU(2) groups.

Similar operations may be performed in two dimensions. Instead of the group SO(4) we now have to deal with a single SU(2) group. The free-energy density in this case becomes

$$L_l=\frac{1}{2}K_l\left[(\partial_i q)^2-\frac{2l(l+1)}{3}q^2\mathrm{Tr}\left[\mathcal{U}^\dagger\partial_i\mathcal{U}-\frac{i\kappa}{2}\epsilon_{ij}\mathcal{U}^\dagger\sigma_j\mathcal{U}\right]^2\right]+\frac{1}{2}r_lq^2\,. \tag{B7}$$

The sum over i and j extends over x and y and $\mathcal{U}$ is again a 2×2 unitary matrix.

We are looking for configurations which are local minima of the free energy to describe the system around a defect line. It can be shown that

$$\mathcal{U}(x,y)=\exp\left[-i\frac{\sigma_2}{2}\Phi(x,y)\right], \tag{B8}$$

where

$$\Phi(x,y)=\sum_i\alpha_i\tan^{-1}\frac{y-y_i}{x-x_i} \tag{B9}$$

is a local minimum of the free energy (B6). This particular choice of Φ represents disclination lines with "charge" α_i running in the z direction. The charge of a $-72°$ disclination line is $\frac{1}{5}$. Note that in this representation we can obtain configurations for both dislocations and disclinations. Disclinations and dislocations have a charge with opposite sign in the second SU(2) group.[17] With these expressions we can evaluate the energy of the defect interactions and cores. We define the correlation length ξ by

$$\xi=\left[\frac{K_n}{t}\right]^{1/2}. \tag{B10}$$

The temperature-like variable t is the frustration-corrected mass and is given by

$$-t=r_n+K_n\kappa^2\frac{n(n+2)}{4}\,. \tag{B11}$$

The magnitude q will be constant over most of space except near the defect cores. The length scale over which q will decrease from its constant value to 0 at the defect core is ξ. After inserting the ansatz (B8) into the free-energy density and performing standard manipulations, the defects are found to have an interaction energy F_D given by

$$F_D\propto\xi^2\alpha_i\alpha_j\ln\frac{|r_i-r_j|}{\xi}\,. \tag{B12}$$

With each defect core there is a loss in condensation energy of the amount (this is the E_c)

$$E_c\propto\xi^2\,. \tag{B13}$$

There is, however, no term in the defect-free energy which couples the defect density to the source of frustration. This is a consequence of the fact that we have chosen to examine *parallel* defect lines. This is in contrast to what happens in the case of a superconductor in a magnetic field. In this case there is a term which directly couples the magnetic field to the vortex density even when all the vortex cores run in the same direction. The incommensurate curvature in the present theory prefers instead a bundle of disclination lines running in all directions to relieve the frustration locally.

APPENDIX C: ICOSAHEDRAL SPHERICAL HARMONICS

Table IV shows the character table for the sixty-element icosahedral point group Y.[43] This character table can be used to determine the allowed values of l in an expansion of a particle density $\rho(\mathbf{u})$ defined on S^2 in spherical harmonics,

$$\rho(\mathbf{u})=\sum_{l=0}^{\infty}\sum_{m=-l}^{l}Q_{lm}Y_{lm}(\mathbf{u})\,. \tag{C1}$$

Although these results are familiar to many investigators, we present the derivation here for completeness.

The set of spherical harmonics for a given l form a $(2l+1)$-dimensional irreducible representation of the group of proper rotations, SO(3). These basis functions, in general, lead to a *reducible* representation of the icosahedral point group. The number of times, a_R, a particular icosahedral irreducible representation, R, will occur is given by[44]

$$a_R(l)=\frac{1}{60}\sum_{(g\in Y)}^{g}\chi_R(g)\chi_l(g)\,. \tag{C2}$$

TABLE IV. Character table for the icosahedral point group.

Y	E	$12\mathcal{C}_5$	$12\mathcal{C}_5^2$	$20\mathcal{C}_3$	$15\mathcal{C}_2$
A	1	1	1	1	1
F_1	3	τ	τ^{-1}	0	-1
F_2	3	τ^{-1}	τ	0	-1
G	4	-1	-1	1	0
H	5	0	0	-1	1

Here, $\chi_R(g)$ are the characters of the group element g in the representation R (see Table IV), and $\chi_l(g)$ are the corresponding characters in the reducible representation generated by $\{Y_{lm}(\theta,\phi),\ m=-l,\ldots,l\}$. If we represent a group element $g\in Y$ by an axis $\mathbf{n}$ and an angle of rotation θ, $g\equiv(n,\theta)$, we have

$$\chi_l(\mathbf{n},\theta)=\frac{\sin[(l+\frac{1}{2})\theta]}{\sin(\frac{1}{2}\theta)}\ . \tag{C3}$$

The rotation angles for the various classes of Y are $\theta=0$ ($\mathscr{C}_0$), $\theta=2\pi/5$ ($\mathscr{C}_5$), $\theta=4\pi/5$ ($\mathscr{C}_5^2$), $\theta=2\pi/3$ ($\mathscr{C}_3$), and $\theta=\pi/2$ ($\mathscr{C}_2$).

The general formula for a particular Fourier coefficient in the expansion (C1) is

$$Q_{lm}=\frac{1}{4\pi}\int d\Omega_{\hat{\mathbf{u}}}Y_{lm}^*(\hat{\mathbf{u}})\rho(\hat{\mathbf{u}})\ , \tag{C4}$$

where the integration is over solid angles on S^2. Suppose $\rho(\hat{\mathbf{u}})$ represents some distribution of points on S^2 with an icosahedral symmetry. Expanding $Y_{lm}^*(\hat{\mathbf{u}})$ in the basis functions appropriate to the irreducible representations of Y, it is straightforward to show that Q_{lm} can only be nonzero if the unit representation A occurs at least once in this expansion. Using Eqs. (C2) and (C3), we have

$$a_A(l)=\frac{1}{60}\left[2l+1+12\frac{\sin[(l+\frac{1}{2})(2\pi/5)]}{\sin(2\pi/5)}+12\frac{\sin[(l+\frac{1}{2})(4\pi/5)]}{\sin(4\pi/5)}+20\frac{\sin[(l+\frac{1}{2})(2\pi/3)]}{\sin(2\pi/3)}+30\frac{\sin[(l+\frac{1}{2})(\pi/2)]}{\sin(\pi/2)}\right]. \tag{C5}$$

Evaluating this formula for different l, we find that $a_A(l)$ is only nonzero for $l=0$, 6, 10, 12, 15, 16, 18, 20, 22, 24, 26, 28, 30, and for all $l>30$. As discussed in Ref. 17, the allowed values of n in an expansion of a density with the symmetry of $\{3,3,5\}$ in *hyperspherical* harmonics are exactly twice these l values.

[1]G. S. Cargill III, in *Solid State Physics,* edited by H. Ehrenreich, F. Seitz, and D. Turnbull (Academic, New York, 1975), Vol. 30, p. 227.

[2]T. Ichikawa, Phys. Status Solidi A **19**, 707 (1973).

[3]P. K. Leung and J. C. Wright, Philos. Mag. **30**, 185 (1974).

[4]J.-P. Lauriat, J. Non-Cryst. Solids **55**, 77 (1983).

[5]See, e.g., J. D. Weeks, Philos. Mag. **35**, 1345 (1977).

[6]R. Zallen, *The Physics of Amorphous Solids* (Wiley, New York, 1983).

[7]K. Kimura and F. Yonezawa, in *Topological Disorder in Condensed Matter,* edited by F. Yonezawa and T. Ninomiga (Springer, Berlin, 1983).

[8]F. C. Frank, Proc. R. Soc. London, Ser. A **215**, 43 (1952).

[9]P. J. Steinhardt, D. R. Nelson, and M. Ronchetti, Phys. Rev. Lett. **47**, 1297 (1981); Phys. Rev. B **28**, 784 (1983).

[10]J. H. Perepezko and J. S. Paik, J. Non-Cryst. Solids **61&62**, 113 (1984).

[11]M. R. Hoare, Adv. Chem. Phys. **40**, 49 (1979).

[12]D. Shechtman, I. Blech, D. Gratias, and J. W. Cahn, Phys. Rev. Lett. **53**, (1984).

[13]J. F. Sadoc, J. Phys. (Paris) Colloq. **41**, C8-326 (1980); see also J. F. Sadoc, J. Phys. (Paris) Lett. **44**, L707 (1983).

[14]D. R. Nelson, Phys. Rev. Lett. **50**, 982 (1983); Phys. Rev. B **28**, 5515 (1983).

[15]J. P. Sethna, Phys. Rev. Lett. **51**, 2198 (1983); Phys. Rev. B **31**, 6278 (1985).

[16]F. C. Frank and J. S. Kasper, Acta Crystallogr. **11**, 184 (1958); **12**, 483 (1959).

[17]D. R. Nelson and M. Widom, Nucl. Phys. B **240**, [FS12], 113 (1984).

[18]M. Bander and C. Itzykson, Rev. Mod. Phys. **38**, 330 (1966).

[19]R. Mosseri and J. F. Sadoc, J. Phys. (Paris) Lett. **45**, L827 (1984).

[20]J. F. Sadoc and R. Mosseri, in *Amorphous Materials,* edited by V. Vitek (American Institute of Metallurgical Engineering, New York, 1983), p. 111.

[21]By an "extreme" type-II superconductor, we mean that H_{c1} is depressed down to $H\simeq 0$.

[22]See, e.g., M. Tinkham, *Introduction to Superconductivity* (McGraw-Hill, New York, 1975).

[23]J. P. Straley, Phys. Rev. B **30**, 6592 (1984).

[24]J. P. Straley (unpublished).

[25]J. F. Sadoc and R. Mosseri, Philos. Mag. B **45**, 467 (1982).

[26]A brief summary of this work was presented in S. Sachdev and D. R. Nelson, Phys. Rev. Lett. **53**, 1947 (1984).

[27]See, e.g., H. E. Stanley, *Introduction to Phase Transitions and Critical Phenomena* (Oxford University Press, New York, 1971).

[28]J. W. Cahn, Acta Metall. **9**, 795 (1961); **10**, 179 (1962); J. E. Hilliard, in *Phase Transformations,* edited by H. I. Aronson (American Society for Metals, Cleveland, 1970).

[29]D. Turnbull and B. G. Bagley, in *Treatise on Solid State Chemistry,* edited by N. B. Hannay (Plenum, New York, 1975), Vol. 5.

[30]N. Connell, W. Paul, and R. J. Tempkin, Adv. Phys. **22**, 581 (1973).

[31]R. J. Temkin, Solid State Commun. **15**, 1325 (1974); N. J. Shevchik and W. Paul, J. Non-Cryst. Solids **13**, 1 (1973/74).

[32]G. A. N. Connell and R. J. Temkin, Phys. Rev. B **9**, 5323 (1974).

[33]M. H. Brodsky, D. P. DiVincenzo, R. Mosseri, and J. F. Sadoc, in Proceedings of the 17th Conference on the Physics of Semiconductors, San Francisco, 1984 (unpublished). This reference was cited incorrectly in Ref. 26.

[34]See, e.g., V. J. Emery and J. Axe, Phys. Rev. Lett. **40**, 1507 (1978).

[35]See, e.g., Refs. 25 and 14.

[36]*CRC Standard Mathematical Tables,* 18th ed. (Chemical Rubber Co., Cleveland, 1970), pp. 15 and 16.

[37]F. Spaepen and D. R. Nelson (unpublished).

[38]R. Collins, in *Phase Transitions and Critical Phenomena,* edited by C. Domb and M. S. Green (Academic, New York,

1972), Vol. II.
[39]D. M. Brink and G. R. Satchler, *Angular Momentum* (Clarendon, Oxford, 1968).
[40]See, e.g., the discussion in P. DuVal, *Homographies, Quaterions, and Rotations* (Oxford University Press, New York, 1964).
[41]L. C. Biedenharn, J. Math. Phys. **2**, 433 (1961).
[42]S. Meiboom, J. P. Sethna, P. W. Anderson, and W. F. Brinkman, Phys. Rev. Lett. **46**, 216 (1981); S. Meiboom, M. Sammon, and W. F. Brinkman, Phys. Rev. A **27**, 438 (1983).
[43]See, e.g., E. B. Wilson, Jr., T. C. Decius, and P. C. Cross, *Molecular Vibrations* (McGraw-Hill, New York, 1955), p. 330. There is a misprint in the entry for the class C_2 in the five-dimensional representation G.
[44]See, e.g., L. D. Landau and E. M. Lifshitz, *Quantum Mechanics* (Pergamon, New York, 1977).

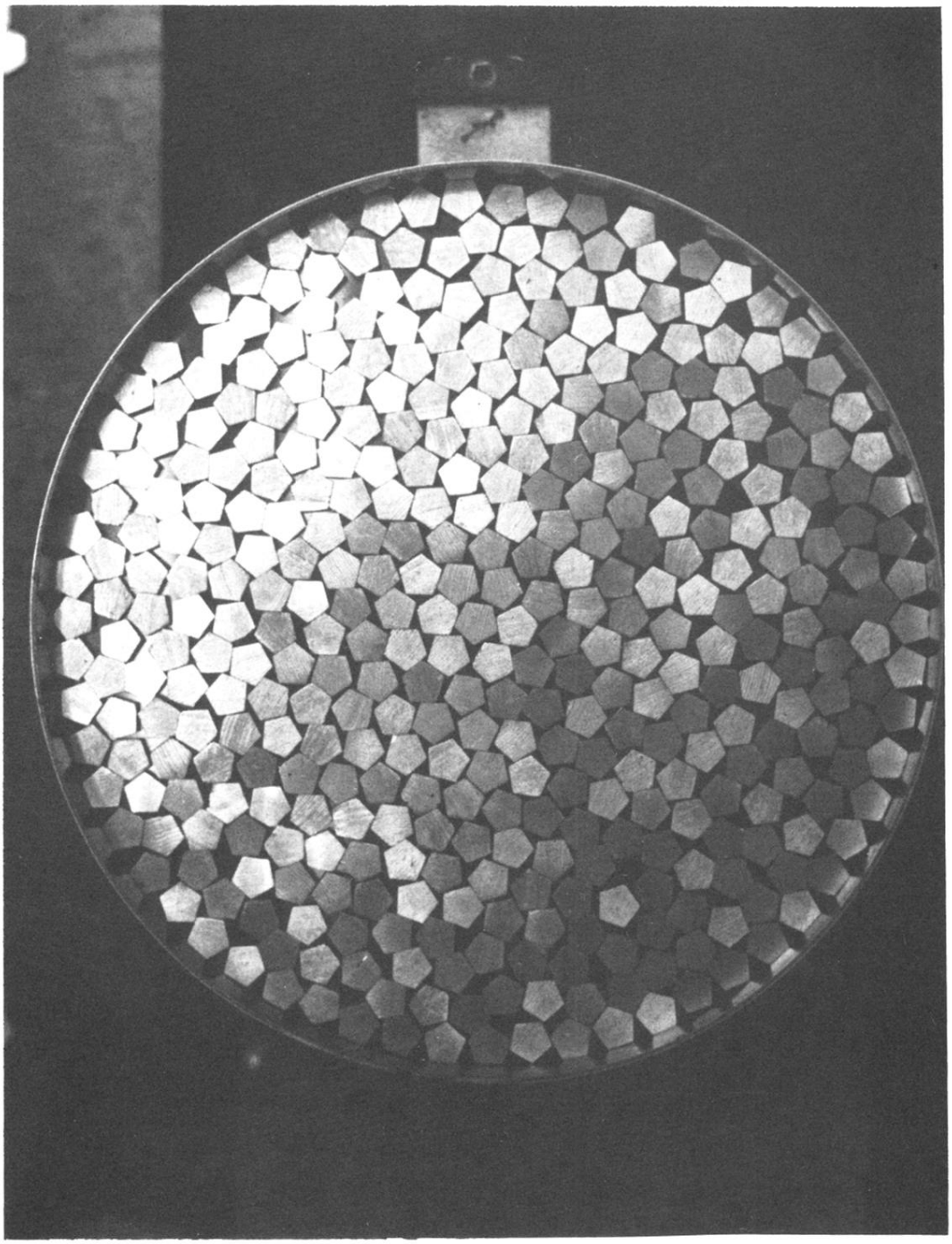

FIG. 3. Snapshot of a configuration obtained by "annealing" a high-density "liquid" of small aluminum pentagons. This configuration was obtained by gradually increasing the density of pentagons in a vibrating-shake-table apparatus (Ref. 37).